Check for updates

Received: 28 April 2022 | Revised: 25 November 2022 | Accepted: 9 January 2023

DOI: 10.1002/suco.202200423

ARTICLE

fib CEB-FIP WILEY

Shear and interface shear of semi-precast slabs with lattice girders under monotonic loading

Matthias Hillebrand | **Josef Hegger**

RWTH Aachen University, Institute of Structural Concrete, Aachen, Germany

Correspondence
Matthias Hillebrand, RWTH Aachen University, Institute of Structural Concrete, Mies-van-der-Rohe, 52074, Aachen, Germany.
Email: mhillebrand@imb.rwth-aachen.de

Funding information
AiF Arbeitsgemeinschaft industrieller Forschungsvereinigungen "Otto von Guericke" e.V., Grant/Award Number: 20580N

Abstract

Semi-precast slabs, where lattice girders serve both as reinforcement in the construction and in the final state, are characterized by a high flexibility and cost efficiency. Due to their technical and economic advantages, they are widely employed in constructions all over the world. In Germany, for example, they are used in about 70% of all floor slabs. To address this economic potential and to improve the design concept for shear and interface shear, theoretical and experimental investigations were conducted at the Institute of Structural Concrete (IMB), RWTH Aachen University. In addition to presenting the general structural behavior of the 16 tests, particular attention is paid to the increase in shear and interface shear resistance at the inner support of continuous slabs and the positive influences of the investigated support detail. The findings illustrate further potential for optimization under monotonic loading, which will also have a positive effect on the fatigue behavior under cyclic loading.

KEYWORDS

experimental investigations, interface shear, lattice girder, precast concrete, reinforced concrete, semi-precast slab, shear

1 | INTRODUCTION

The lower part of a semi-precast reinforced concrete slab with lattice girders is produced in a precast plant and then completed with a layer of in-situ concrete on the construction site. The lattice girders serve both as reinforcement for transport and assembling and as reinforcement in the final state. Semi-precast slabs are characterized by a high flexibility and cost efficiency. They combine the advantages of precast and cast-in-place concrete construction, since the precast slab eliminates the need for formwork on the one hand, and the lattice girders enable an almost monolithic structural behavior on the other hand. Prefabrication shortens construction times and reduces errors at the construction site. Due to the technical and economic advantages of the precast construction method, an estimated 70% of all floor slabs in building construction in Germany are executed as semi-precast slabs with lattice girders.[1]

While the semi-precast slabs are single-span slabs in the construction phase, statically indeterminate continuous slab

Discussion on this paper must be submitted within two months of the print publication. The discussion will then be published in print, along with the authors' closure, if any, approximately nine months after the print publication.

This is an open access article under the terms of the Creative Commons Attribution License, which permits use, distribution and reproduction in any medium, provided the original work is properly cited.
© 2023 The Authors. *Structural Concrete* published by John Wiley & Sons Ltd on behalf of International Federation for Structural Concrete.

17517648, 0, Downloaded from https://onlinelibrary.wiley.com/doi/10.1002/suco.202200423 by Rwth Aachen Hochschulbibliothe, Wiley Online Library on [27/02/2023]. See the Terms and Conditions (https://onlinelibrary.wiley.com/terms-and-conditions) on Wiley Online Library for rules of use; OA articles are governed by the applicable Creative Commons License

systems are generated by the layer of in situ concrete. The favorable influence of a continuous system on the shear and interface shear resistance, as has already been determined for monolithic slabs without shear reinforcement, with a low shear reinforcement ratio and beams with shear reinforcement,[2,3] has not yet been investigated and is consequently not considered in the current design approaches for semi-precast slabs with lattice girders.

Semi-precast slabs can generally be used for both monotonic and cyclic loading. For fatigue design, *S-N*-curves for different lattice girder types have been developed.[4,5] However, more investigations are still missing for the improvement of the design concept since the current design approach for shear fatigue leads to high shear reinforcement ratios and thus to uneconomical results. To analyze the behavior under cyclic loading, initially, a closer look at the structural behavior of semi-precast slabs under monotonic loading is necessary.

To address this economic potential and to improve the design concept for shear and interface shear in semi-precast slabs with lattice girders, both theoretical and experimental investigations were conducted at the Institute of Structural Concrete (IMB), RWTH Aachen University.

This paper presents the tests with monotonic loading and the results obtained from these tests. In addition, the tests serve as a basis for the cyclic tests, which will be documented in a further publication. The investigations described in this paper are conducted during a research program initiated by the Research Association of the German Concrete and Precast Industry e.V. and funded by the German Federation of Industrial Research Association (AiF, IGF number 20580N) and the Federal Ministry for Economic Affairs and Climate Action based on a resolution of the German Bundestag.

2 | THEORETICAL BACKGROUND

2.1 | Lattice girders

In semi-precast constructions, lattice girders act as interface reinforcement between the precast element and the in situ concrete and depending on the design, can also be used as shear or punching reinforcement (Figure 1). Due to their special geometry, the design of lattice girders in Germany is defined in technical approvals (TA) for lattice girders. A selection of different lattice girder types is shown in Figure 1d–f. A comprehensive overview of lattice girders and their use in semi-precast slabs is given in Furche et al.[1]

The lattice girder in Figure 1e, known as EQ from Filigran[6] or KTS from Badische Drahtwerke,[7] is designed for high shear resistance. Due to this fact and its applicability, this type of lattice girder was selected for the investigations presented here. In addition, this lattice girder is approved for use under cyclic loading and can therefore also be used for fatigue tests. A review of further research on lattice girders and in particular their use under cyclic loading is presented in Hillebrand et al.[5]

2.2 | Shear

Lattice girders can be classified as shear reinforcement according to DIN EN 1992-1-1 (EC2),[8,9] if the design and construction rules for shear links, ladders or inclined bars are fulfilled. The design for shear according to the TA[6,7] follows the design rules according to EC2. For shear-optimized lattice girders (Figure 1e), both the cross-sections of both the diagonal ($90° \geq \alpha_1 \geq 45°$) and vertical bars ($\alpha_2 = 90°$) may be accounted for in the calculation of shear resistance given in Equation (1).

$$V_{Ed} \leq V_{Rd,sy} = \frac{A_{sw}}{s} \cdot f_{yd} \cdot z \cdot \sum\nolimits_{i \geq 1} (\cot\theta + \cot\alpha_i) \cdot \sin\alpha_i \tag{1}$$

Where f_{yd} is the design value of the yield strength of the reinforcing steel; z is the inner lever arm; θ is the inclination of the compression strut; α_i is the inclination of shear reinforcement; A_{sw} is the cross-sectional area of shear reinforcement; s is the spacing of the shear reinforcement measured along the longitudinal axis of the member.

In Germany, the compression strut inclination is limited by Equation (2) for non-prestressed members according to the German national annex to EC2 (NA(D)).[9] The inclination θ depends in particular on the concrete contribution $V_{Rd,cc}$ (Equation (3)). Furthermore, the maximum resistance is reduced to $V_{Rd,max,GT} = 0.3 \cdot V_{Rd,max}$ according to NA(D)[9] if lattice girders are installed as shear reinforcement.

$$1.0 \leq \cot\theta \leq \frac{1.2}{1 - V_{Rd,cc}/V_{Ed}} \leq 3.0 \tag{2}$$

$$V_{Rd,cc} = 0.24 \cdot f_{ck}^{1/3} \cdot b \cdot z \tag{3}$$

2.3 | Interface shear

DIN EN 1992-1-1 + NA(D) (EC2 + NA(D)) uses an additive approach of adhesion, friction, and interface reinforcement for the resistance in the interface[8,9]:

17517648, 0, Downloaded from https://onlinelibrary.wiley.com/doi/10.1002/suco.202200423 by Rwth Aachen Hochschulbibliothe, Wiley Online Library on [27/02/2023]. See the Terms and Conditions (https://onlinelibrary.wiley.com/terms-and-conditions) on Wiley Online Library for rules of use; OA articles are governed by the applicable Creative Commons License

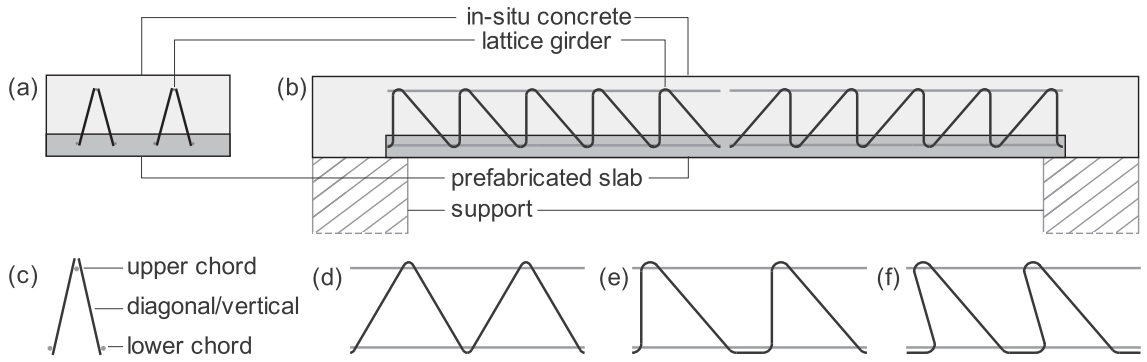


FIGURE 1 (a) Cross-section and (b) longitudinal section of a semi-precast slab; (c) cross-section of lattice girder; longitudinal section of lattice girders optimized for (d) interface shear, (e) shear and (f) punching

TABLE 1 Factors for interface resistance depending on the surface roughness

Surface	Adhesion c	Friction μ	Strength reduction factor for concrete cracked in shear ν
Indented	0.5	0.9	0.7
Rough	0.4	0.7	0.5
Smooth	0.2	0.6	0.2
Very smooth	0	0.5	0.2

$$\frac{V_{\mathrm{Ed}}}{z \cdot b_i} \le \nu_{\mathrm{Rdi}} \tag{4}$$

$$\nu_{\mathrm{Rdi}} = c \cdot f_{\mathrm{ctd}} + \mu \cdot \sigma_n + \sum\nolimits_{i \ge 1} \rho_{w,i} \cdot f_{yd} \cdot (1.2\mu \cdot \sin\alpha_i + \cos\alpha_i) \le 0.5 \cdot \nu \cdot f_{\mathrm{cd}} \tag{5}$$

The factors c, μ, and ν depend on the interface roughness and can be taken from Table 1 according to EC2 + NA(D). The additive approach is limited by the concrete strength of precast or in situ concrete, where the lower value is decisive. For interface reinforcement, the diagonal and vertical bars may be considered for shear lattice girders EQ/KTS, considering their angle of inclination ($90° \ge \alpha_1 \ge 45°$ and $\alpha_2 = 90°$). The optimized verification of shear interface according to the TA is performed analogously to EC2 + NA(D).

2.4 | Shear slenderness

All experimental investigations on the shear resistance of semi-precast slabs with lattice girders have so far been carried out exclusively on single-span slabs. The design equations for shear and interface shear were derived and verified with these tests and transferred to continuous systems without any adjustments.

However, the shear resistance of beams and slab members is significantly influenced by shear slenderness.[10–17] With an increasing shear slenderness, the shear capacity of the member decreases. The shear slenderness is generally described by Equation (6). For single-span elements under concentrated loads, the shear slenderness can be simplified depending on the distance a between the load and the support and the effective depth d using Equation (7).

$$\lambda = \frac{M}{V \cdot d} \tag{6}$$

$$\lambda = \frac{a}{d} \tag{7}$$

For the same a/d ratios, the shear slenderness at internal supports of continuous elements is significantly smaller than the shear slenderness for single-span elements and end supports (Figure 2a). This implies also a larger shear resistance due to the direct transfer of the compression struts to the support. The results of recent investigations on slab stripes without shear reinforcement[2,18] confirm these relationships (Figure 2b).

Investigations on continuous beams with shear reinforcement[19–24] also confirm the increase in shear resistance with decreasing shear slenderness. However, this effect is decreasing to zero with increasing shear reinforcement ratio. The positive influence of a reduced shear slenderness for continuous members compared to single-span members is not taken into account in current design concepts for semi-precast slabs[6–9] which usually have small and medium shear reinforcement ratios.

17517648, 0, Downloaded from https://onlinelibrary.wiley.com/doi/10.1002/suco.202200423 by Rwth Aachen Hochschulbibliothe, Wiley Online Library on [27/02/2023]. See the Terms and Conditions (https://onlinelibrary.wiley.com/terms-and-conditions) on Wiley Online Library for rules of use; OA articles are governed by the applicable Creative Commons License

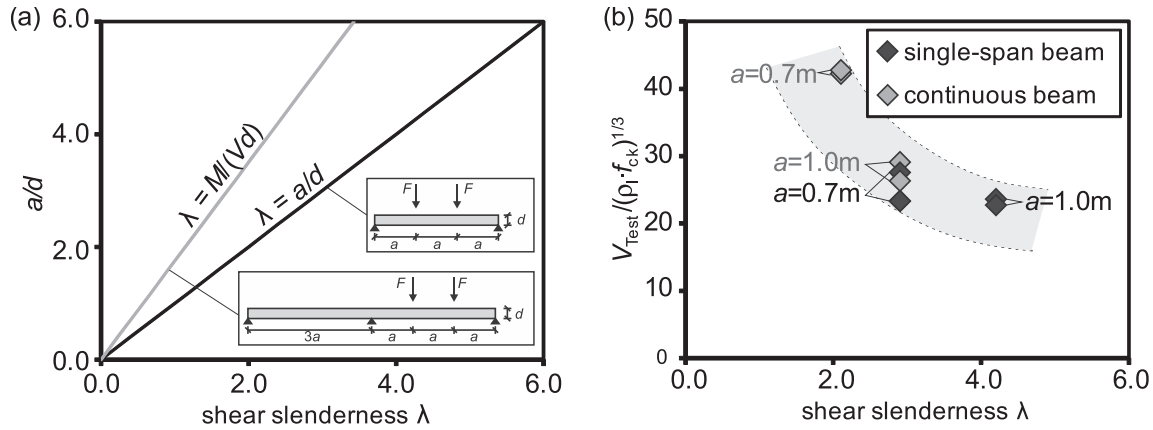


FIGURE 2 Relationship between shear slenderness λ and (a) a/d ratio and (b) shear resistance of single-span and continuous beams (according to Adam et al.[2,18])

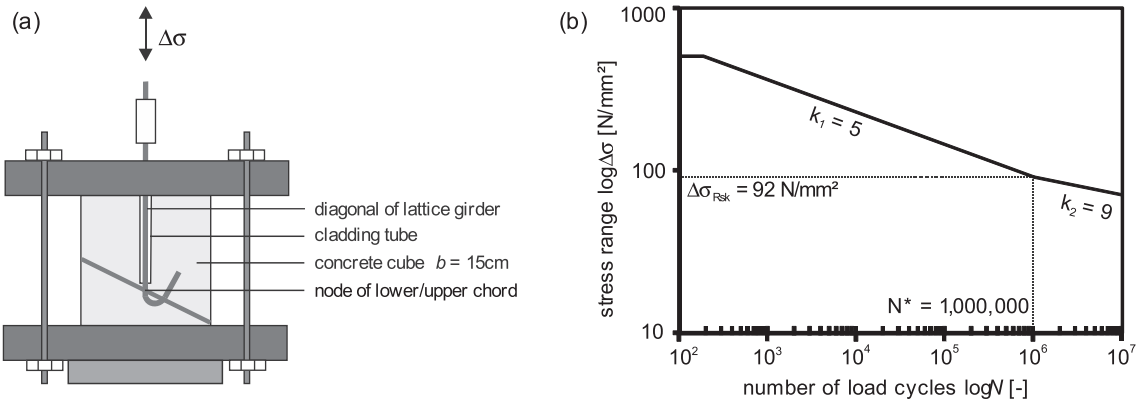


FIGURE 3 (a) Schematic depiction of fatigue test setup; (b) Assessed S–N curve for lattice girders in the latest technical approvals[6,7]

3 | EXPERIMENTAL INVESTIGATIONS

3.1 | General

The experimental investigations are an extension to the investigations of Hillebrand et al. and Hegger and Wieneke,[5,25] where the fatigue behavior of small size tests and slab specimens was investigated. For the small size tests the welded nodes as a critical part of the lattice girder diagonal were cast in concrete cubes (Figure 3a). Cyclic loading was applied to the diagonals with constant stress ranges. Based on these tests an S–N curve was derived (Figure 3b). Subsequently, the fatigue behavior of 14 slab specimens was investigated. The measured stress ranges in the lattice girder diagonals were significantly larger than the permitted stress ranges and at the same time lower than the stress ranges calculated according to the current design concept. Failure of the slabs due to fatigue fractures of the lattice girders often occurred only after large numbers of load cycles despite large stress ranges. However, due to the lack of monotonic reference tests and in part highly scattered test results in combination with changing failure modes of the interface and the lattice girders, it was not possible to derive a conclusive design concept.

Therefore, in addition to the monotonic reference tests, a major focus of the new investigations was the determination of the measured stress ranges. An aim was also to investigate new issues such as the influence of the shear slenderness on shear capacity. As an extended investigation on shear and interface shear behavior of semi-precast slabs with lattice girders, 32 test specimens were manufactured at the Institute of Structural Concrete (IMB). Sixteen slabs were tested under monotonic loading and 16 identical slabs were subjected to cyclic loading. The tests were divided into two series according to the slab depth. Table 2 gives an overview of the test program and the selected parameters. More details are given in Sections 3.2 and 3.3.

17517648, 0, Downloaded from https://onlinelibrary.wiley.com/doi/10.1002/suco.202200423 by Rwth Aachen Hochschulbibliothe, Wiley Online Library on [27/02/2023]. See the Terms and Conditions (https://onlinelibrary.wiley.com/terms-and-conditions) on Wiley Online Library for rules of use; OA articles are governed by the applicable Creative Commons License

TABLE 2 Test program

Tests		Support condition		Shear reinforcement ratio		Concrete strength		Surface roughness [mm]	Depth [cm]		Ø longitudinal reinforcement [mm]	
stat.	cycl.	s.span	cont.	low	high	C25	C50		16	34	15	20
Series 3	EG15a	X		X		X		alm. rough	X		X	
	EG15b		X	X		X		alm. rough	X		X	
	EG16c	X		X		X		alm. rough	X		X	
	EG16d		X	X		X		alm. rough	X		X	
	EG17a	X			X	X		alm. rough	X		X	
	EG17b		X		X	X		alm. rough	X		X	
	EG18c	X			X	X		alm. rough	X		X	
	EG18d		X		X	X		alm. rough	X		X	
	EG19a	X		X		X		v. smooth	X		X	
	EG19b		X	X		X		v. smooth	X		X	
	EG20c	X		X		X		v. smooth	X		X	
	EG20d		X	X		X		v. smooth	X		X	
	EG21a	X			X		X	alm. rough	X		X	
	EG21b		X		X		X	alm. rough	X		X	
	EG22c	X			X		X	alm. rough	X		X	
	EG22d		X		X		X	alm. rough	X		X	
Series 4	EG23a	X		X		X		alm. rough		X		X
	EG23b		X	X		X		alm. rough		X		X
	EG24c	X		X		X		alm. rough		X		X
	EG24d		X	X		X		alm. rough		X		X
	EG25a	X			X	X		alm. rough		X		X
	EG25b		X		X	X		alm. rough		X		X
	EG26c	X			X	X		alm. rough		X		X
	EG26d		X		X	X		alm. rough		X		X
	EG27a	X			X		X	alm. rough		X		X
	EG27b		X		X		X	alm. rough		X		X
	EG28c	X			X		X	alm. rough		X		X
	EG28d		X		X		X	alm. rough		X		X
	EG29a	X		X		X		alm. rough		X		X*
	EG29b		X	X		X		alm. rough		X		X
	EG30c	X		X		X		alm. rough		X		X*
	EG30d		X	X		X		alm. rough		X		X

Note: a: single-span slab with monotonic loading; b: continuous slab with monotonic loading; c: single-span slab with cyclic loading; d: continuous slab with cyclic loading; s.span, single-span slab ($\lambda = 4.0$); cont., continuous slab ($\lambda = 2.5$); low, low shear reinforcement ratio (2 rows); high, high shear reinforcement ratio (4 rows); alm. rough, almost rough ($R_t \leq 1.5$ mm, Section 3.2.2); v.smooth, very smooth; *, single-span slab with top longitudinal reinforcement.

3.2 | Test specimens

3.2.1 | Design of the test specimens

The test specimens of series 3 had a total slab depth of 16 cm. According to the TA, this is the minimum depth of a slab with lattice girders when shear reinforcement is required. The depth of the precast slabs was designed to be 6 cm, which corresponds to the minimum depth for cyclic loads according to TA. The in-situ concrete had a depth of 10 cm. The test specimens of series 4 had a depth of 34 cm, with a depth of the precast slab of 7 cm and depth of the in-situ concrete of 27 cm. The width of all slabs was 85 cm, due to the test rig and in accordance

17517648, 0, Downloaded from https://onlinelibrary.wiley.com/doi/10.1002/suco.202200423 by Rwth Aachen Hochschulbibliothe, Wiley Online Library on [27/02/2023]. See the Terms and Conditions (https://onlinelibrary.wiley.com/terms-and-conditions) on Wiley Online Library for rules of use; OA articles are governed by the applicable Creative Commons License

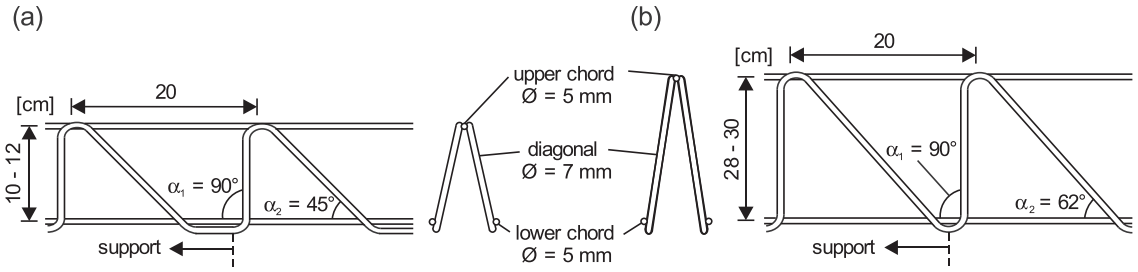


FIGURE 4 Geometries of lattice girders in (a) series 3 and (b) series 4

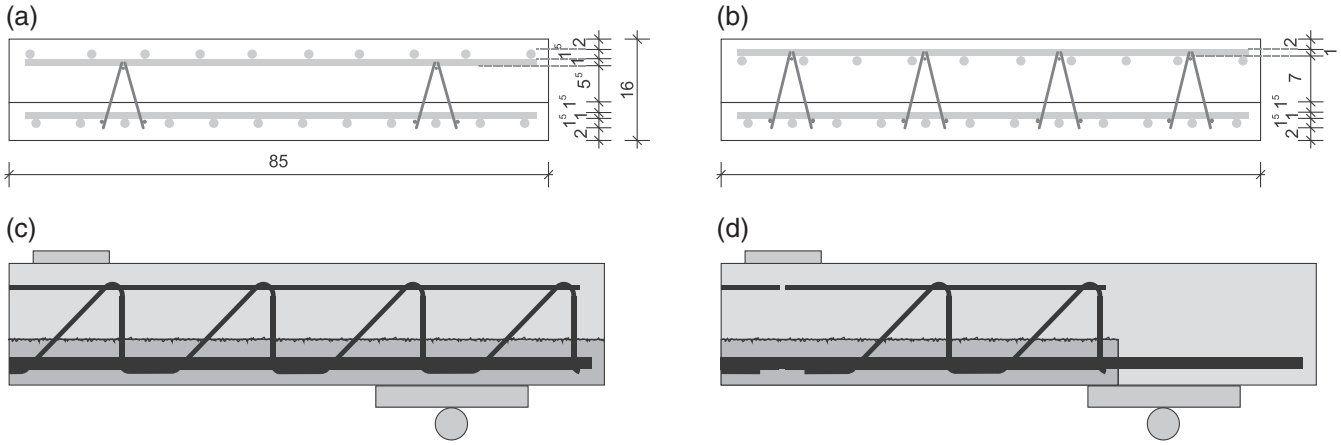


FIGURE 5 Arrangement of the upper transverse and longitudinal reinforcement for (a) moderate loading and (b) high loading; (c) detailing of support in Hillebrand et al. and Hegger and Wieneke[5,25]; (d) detailing of support in current investigation

with the test specimens in the previous project (test series 1 and 2).

The lattice girders KTS from Badische Drahtwerke[7] and EQ from Filigran,[6] which are identical in construction, were used as shear and interface shear reinforcement (Figure 4). The test specimens were either designed with two rows of lattice girders (low shear or interface shear reinforcement ratio, $\rho_w = 1.8$ ‰) or with four rows of lattice girders (high shear reinforcement ratio, $\rho_w = 3.6$‰).

When using lattice girders as interface or shear reinforcement under moderate loading (low degree of shear reinforcement), the upper transverse and longitudinal reinforcement may be stacked on the lattice girders according to TA[6,7] (Figure 5a). For the slabs with high loading, the upper longitudinal reinforcement must be placed at the level of the upper chord of the lattice girders. The transverse reinforcement may still be placed above the lattice girder (Figure 5b). To maintain the required concrete cover, the height of the lattice girders was reduced in the tests with two rows of lattice girders due to this reinforcement arrangement. In result, the depths of the lattice girders for the series 3 slabs were 10 cm (moderate loading) and 12 cm (high loading), respectively. For the series 4 slabs, the depths were 28 cm and 30 cm, respectively. In principle, the upper reinforcement was only installed in the area of the inner support of the single-span slabs with cantilever (representing continuous slab systems). To investigate the influence of this upper bending reinforcement on the crack behavior and resulting load-bearing capacities, the single-span slabs EG29a and EG30c were also equipped with upper transverse and longitudinal reinforcement. To avoid flexural failure high-strength bars (S900/1100, $f_y = 900$ N/mm^2, $E_s \approx 190{,}000$ N/mm^2) with Ø15 mm and Ø20 mm were used as longitudinal reinforcement.[26] shows that influences from the use of high-strength flexural reinforcement on the shear capacity can be excluded. Ribbed B500 reinforcing steel was used for the transverse reinforcement. The lattice girders were made of smooth reinforcing steel with a diameter of 5 mm for the upper and lower chords and 7 mm for the vertical and diagonal bars (Figure 4). The average yield strength of the diagonals was $f_y = 520$ N/mm^2 (Table 3).

In the previous project,[5,25] the interface between the prefabricated slab and the in-situ concrete was provided along the entire slab length (Figure 5c). According to the

17517648, 0, Downloaded from https://onlinelibrary.wiley.com/doi/10.1002/suco.202200423 by Rwth Aachen Hochschulbibliothe, Wiley Online Library on [27/02/2023]. See the Terms and Conditions (https://onlinelibrary.wiley.com/terms-and-conditions) on Wiley Online Library for rules of use; OA articles are governed by the applicable Creative Commons License

TABLE 3 Average yield and tensile strength of reinforcement

	Ø [mm]	*n*	f_y [N/mm²]*	f_t [N/mm²]*
Lattice girder: upper chord	5	6	566 (533–575)	612 (597–620)
Lattice girder: vertical/diagonal bar	7	18	520 (511–557)	570 (550–598)
Lattice girder: lower chord	5	12	556 (544–584)	613 (606–614)
Longitudinal reinforcement series 3	15	3	1014 (1010–1018)	1187 (1185–1198)
Longitudinal reinforcement series 4	20	3	982 (972–990)	1196 (1183–1208)

Note: *n*, number of specimens tested; *, mean value and range in tests.

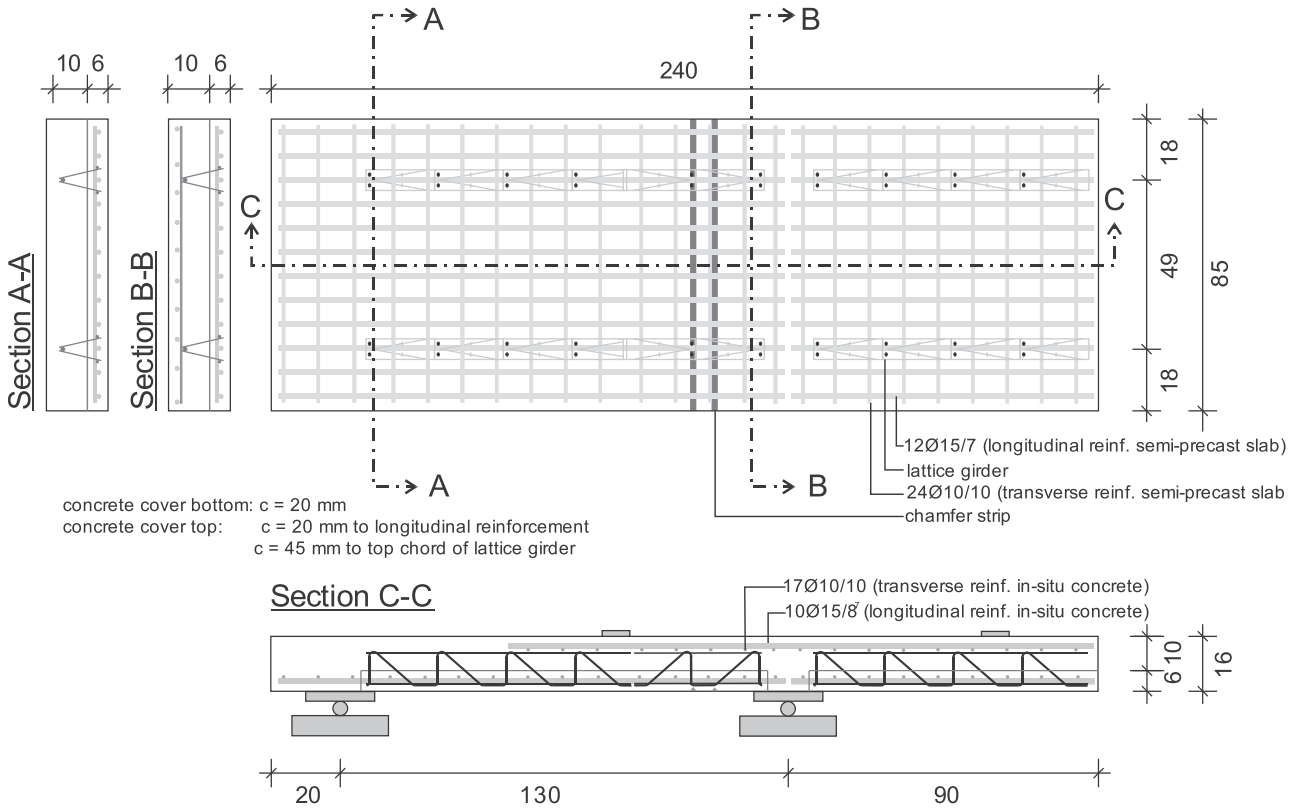


FIGURE 6 Reinforcement of single-span slabs with cantilever EG15b and EG16d

usual construction on site, the precast slab is placed only 3.5 cm onto the support in these tests (Figure 1b), and the lattice girder is only provided within the prefabricated slab. The longitudinal reinforcement protruded from the prefabricated slab into the in situ concrete. In this area, the in situ concrete is poured over the entire slab depth (Figure 5d).

Figure 6 shows the exemplary reinforcement of the slabs EG15b and EG16d. The test report contains a compilation of the reinforcement drawings of all test specimens.[27] Table 4 shows an overview of the dimensions and geometrical parameters of the test specimens.

The same concrete strengths were aspired for the precast slabs and the in situ concrete. The minimum and maximum concrete compressive strength according to the TA (C25/30 and C50/60) were used. The design of the concrete mix is shown in Table 5. The concrete strength was determined on at least three cylinders per slab. The mean strength overall tests were in a range of $f_{cm,cyl} = 21.8$ and 35.1 N/mm² for C25/30 and in a range of $f_{cm,cyl} = 48.8$ and 63.2 N/mm² for C50/60 with a small scatter in each test slab. The slabs were produced consecutively with the tests and the age of the concrete when the slabs were tested was between 7 and 88 days. To keep the influence at a minimum, in all evaluations the concrete strengths of the test day were used. A list of all material properties can be found in the test report.[27]

17517648, 0, Downloaded from https://onlinelibrary.wiley.com/doi/10.1002/suco.202200423 by Rwth Aachen Hochschulbibliothe, Wiley Online Library on [27/02/2023]. See the Terms and Conditions (https://onlinelibrary.wiley.com/terms-and-conditions) on Wiley Online Library for rules of use; OA articles are governed by the applicable Creative Commons License

TABLE 4 Dimensions and geometrical parameters of the test specimens

	Series 3		Series 4	
	Single-span	**continuous**	**Single-span**	**continuous**
Dimensions ($l/b/h$) [cm]	170/85/16	240/85/16	384/85/34	542/85/34
Thickness prefabricated slab/in situ concrete [cm]	6/10	6/10	7/27	7/27
Effective depth d [cm]	13.3	13.3	31.0	31.0
Distance support/load a [cm]	50	50	130	130
Shear slenderness λ [−]	4	2.5	4	2.5
Lattice girder [−]	EQ/KTS	EQ/KTS	EQ/KTS	EQ/KTS
Low shear reinforcement ratio ρ_l [%]	1.8	1.8	1.8	1.8
High shear reinforcement ratio ρ_l [%]	3.6	3.6	3.6	3.6
Longitudinal reinforcement ratio ρ_l [%]	2.0	2.0	2.0	2.0

TABLE 5 Design of concrete mix

	C25/30	**C50/60**
Cement CEM I 42.5 R [kg/m^3]	260	450
Water [kg/m^3]	182	180
Water–cement ratio	0.7	0.4
Superplasticizer [kg/m^3]	3	3
Aggregate with grain size 0–0.2 mm [kg/m^3]	252	232
Aggregate with grain size 0.2–1 mm [kg/m^3]	329	303
Aggregate with grain size 1–2 mm [kg/m^3]	213	196
Aggregate with grain size 2–4 mm [kg/m^3]	213	196
Aggregate with grain size 4–8 mm [kg/m^3]	252	232
Aggregate with grain size 8–16 mm [kg/m^3]	678	624

3.2.2 | Production of the test specimens

All test specimens were produced at the IMB. The reinforcement of a thin (series 3, 16 cm) and a thick (series 4, 34 cm) slab are shown in Figure 7.

Since a rough interface is required by the TA,[6,7] for the test specimens, a mean roughness of little less than $R_t = 1.5$ mm ("almost rough", Table 2) was aimed for, which is slightly below a rough interface according to EC2. For this purpose, the interfaces were roughened by brush stroke after concreting the precast slab. For the test specimens EG19a, EG19b, EG20c, and EG20d, on the other hand, a very smooth interface was planned. In order to investigate the pure resistance of the reinforcement the adhesion and friction were eliminated almost completely by smoothing the fresh concrete and curing the hardened surface with grease. The effectiveness of this work step was already demonstrated in the previous project.[5,25] For each prefabricated slab, the mean roughness depth R_t was measured using the sand patch method according to Kaufmann,[28] which is the standard procedure for this case. Since this method is very user-dependent and sometimes provides scattering results, an additional measurement was conducted using laser technology.[29] Laser measurements were carried out using the ELAtextur measuring device from IWS Messtechnik. Since the measuring device did not fit between the lattice girders on all slabs, the laser measurements were performed on slabs with approximately the same roughness that were additionally produced together with the respective prefabricated slab. Figure 8a provides an overview of all measured surface roughness. For the values given, both the areas between and under the lattice girders were considered according to their percentage of the surface. Since a greased surface can no longer be measured properly, the surface was defined as very smooth for slabs EG19a and EG19b according to the test results of Hillebrand et al. and Hegger and Wieneke.[5,25] Their roughness given in Figure 8a was measured before the grease was applied. An example of the roughened surface can be seen in Figure 8b. Some days after concreting the precast slab, the upper transverse and longitudinal reinforcement was installed for the slabs with cantilever. Finally, the in situ concrete was poured.

3.3 | Test setup

The tests were carried out using the servo-hydraulic testing machine HB5000 from Zwick/Roell at the IMB. The test specimens were supported by two support blocks with steel rollers in order to avoid constraints. The load F was applied over the entire width of the slab. For series 3 slabs with a depth of 16 cm, the load was applied at 0.5 m distance from the support; the

17517648, 0, Downloaded from https://onlinelibrary.wiley.com/doi/10.1002/suco.202200423 by Rwth Aachen Hochschulbibliothe, Wiley Online Library on [27/02/2023]. See the Terms and Conditions (https://onlinelibrary.wiley.com/terms-and-conditions) on Wiley Online Library for rules of use; OA articles are governed by the applicable Creative Commons License

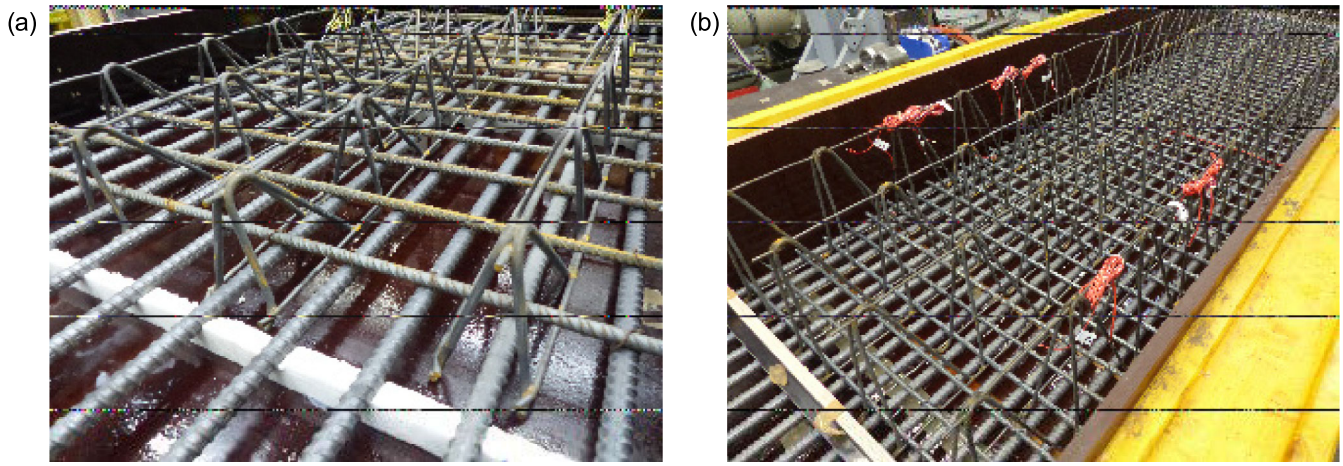


FIGURE 7 Reinforcement of test specimens from (a) series 3 and (b) series 4

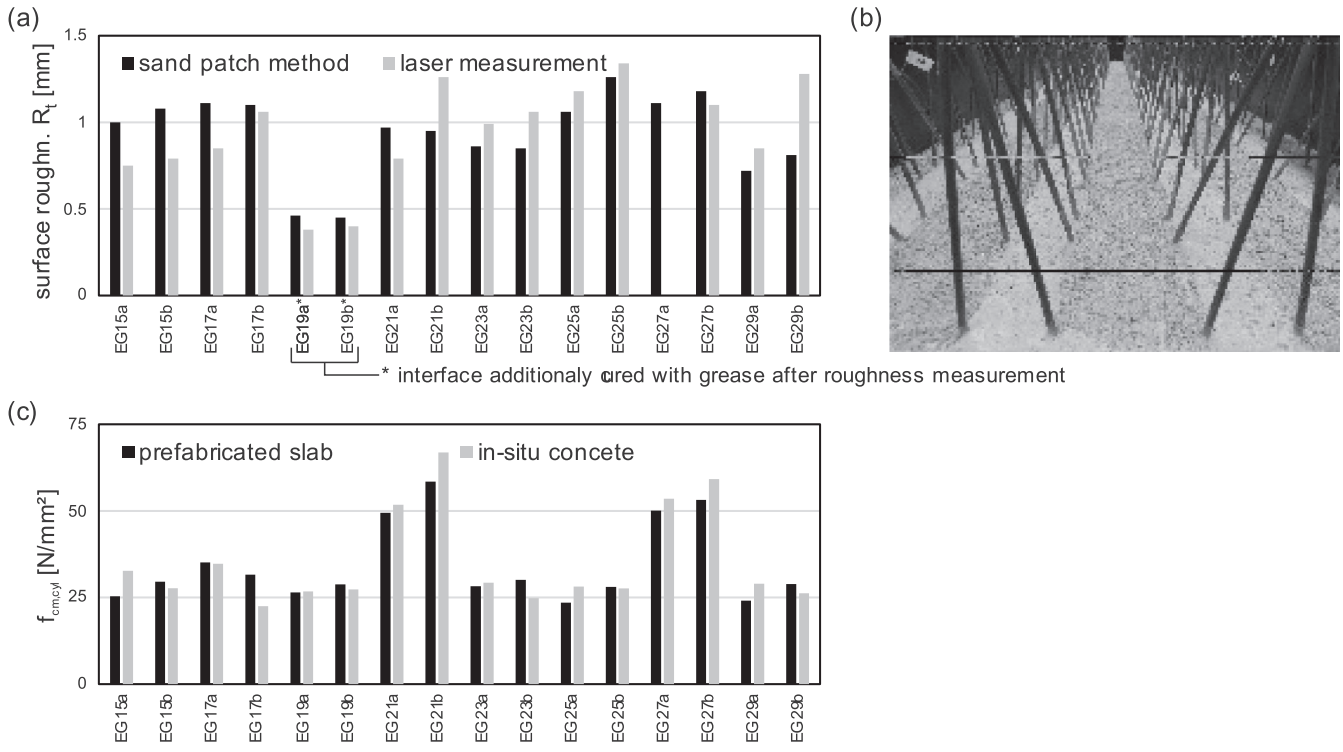


FIGURE 8 Overview of (a) measured roughness R_t, (b) surface roughness of roughened prefabricated slab EG27a and (c) concrete strength of prefabricated slabs and in-situ concrete

load distance for series 4 slabs with a depth of 34 cm was 1.3 m (Figure 9).

The influence of the shear slenderness on the shear resistance was investigated using single-span and continuous slabs with constant load distances a, resulting in a shear slenderness of $\lambda = 4.0$ and $\lambda = 2.5$ (according to Equation (6)), respectively. The slabs designed as single-span slabs with cantilever were loaded with a load F_k at the cantilever that was increased linearly with the test load at the inner span F to achieve a continuous action while keeping the shear slenderness constant throughout the test. The resulting internal forces are shown in Figure 10.

The monotonic loading of the tests was carried out in a displacement-controlled manner at a speed of 0.5 mm/min. Deformations and crack widths as well as strains were continuously measured by the attached

17517648, 0, Downloaded from https://onlinelibrary.wiley.com/doi/10.1002/suco.202200423 by Rwth Aachen Hochschulbibliothe, Wiley Online Library on [27/02/2023]. See the Terms and Conditions (https://onlinelibrary.wiley.com/terms-and-conditions) on Wiley Online Library for rules of use; OA articles are governed by the applicable Creative Commons License

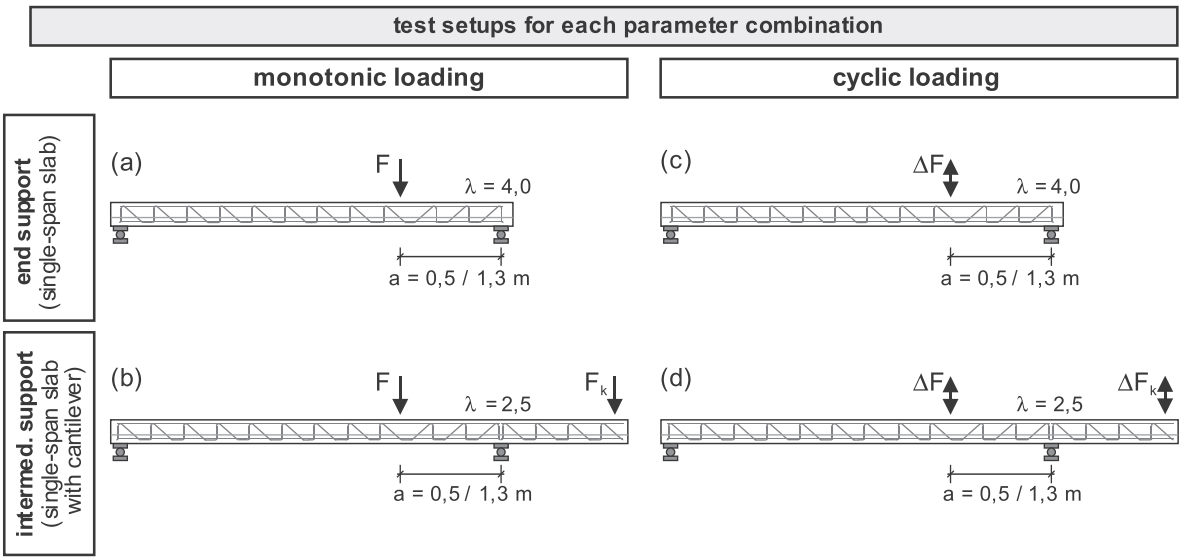


FIGURE 9 Schematic test setups of the monotonic and cyclic tests

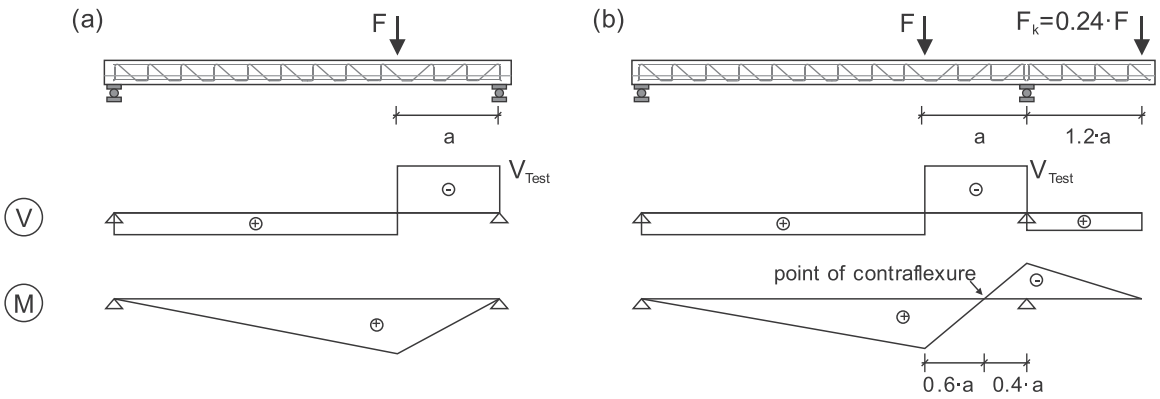


FIGURE 10 Load and internal forces on (a) single-span slab and (b) single-span slab with cantilever

displacement transducers and strain gages (SG; Section 3.4) for the evaluation of the tests.

3.4 | Measurement instrumentation

The continuous recording of the behavior of the slabs during the test was carried out using strain gages and inductive displacement transducers. Figure 11 shows the arrangement of the measurement instrumentation as an example for a series 3 slab. Details of all slabs can be found in the test report.[27]

The SG were attached to the lattice girders (inclined and vertical bars) to record the corresponding strain in the reinforcement. They were located in the areas of the slabs where shear cracks were expected. In addition, a strain gage was attached to the lower longitudinal reinforcement (SL21) just below the load introduction. For the slab with cantilever, a further strain gage (SL22) was provided at the upper longitudinal reinforcement centrally above the inner support. For slabs EG19a, EG19b, EG20c, and EG20d, additional SG were placed at the bottom longitudinal reinforcement (SL23–SL26).

The inductive displacement transducers recorded deflection (W1), interface displacements [horizontal (W2) and vertical (W3)], and crack widths (W4, W5) of the shear cracks. The displacement transducers for determining the crack widths and interface displacement were arranged on one side of the slab.

On the other side, the interface displacement and crack width were determined by digital image correlation (DIC; Figure 11). The evaluation was performed with GOM Correlate.[30]

17517648, 0, Downloaded from https://onlinelibrary.wiley.com/doi/10.1002/suco.202200423 by Rwth Aachen Hochschulbibliothe, Wiley Online Library on [27/02/2023]. See the Terms and Conditions (https://onlinelibrary.wiley.com/terms-and-conditions) on Wiley Online Library for rules of use; OA articles are governed by the applicable Creative Commons License

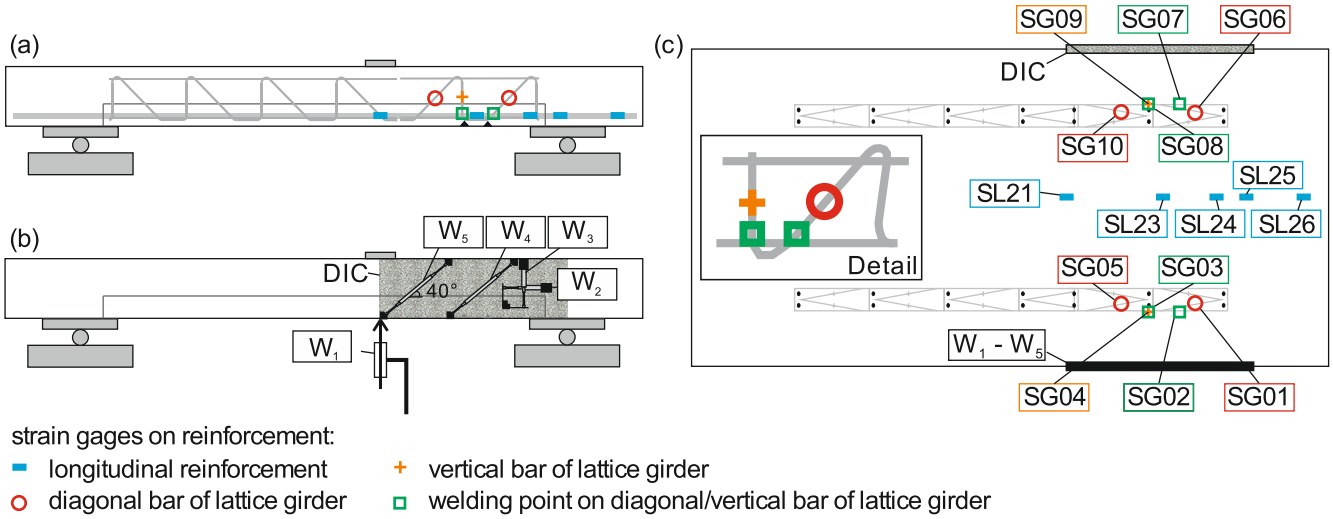
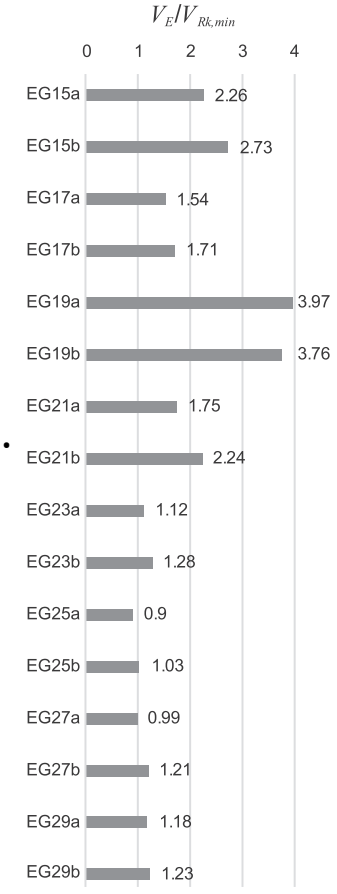


FIGURE 11 Overview of the installed measurement instrumentation for EG20c; (a,b) section/side view; (c) top view with detail of strain gages on lattice girders.

TABLE 6 Overview of loads and calculated load resistances of the monotonic tests

		V_I [kN]	V_E [kN]	$V_{Rk,sy}$ kN]	$V_{Rk,I}$ [kN]	$V_E/V_{Rk,I}$ [−]	$V_E/V_{Rk,fail}$ [−]	Failure type [−]	$V_E/V_{Rk,min}$
• Series 3 (H = 16 cm)	• EG15a	• –	• 253	• 128.6	• 112.1*	• 2.26	• 1.97	• *S*	
	• EG15b	• –	• 321	• 128.6	• 117.4*	• 2.73	• 2.50	• *S*	
	• EG17a	• –	• 288	• 214.0	• 186.6*	• 1.54	• 1.34	• *S*	
	• EG17b	• –	• 293	• 206.3	• 171.2*	• 1.71	• 1.42	• *S*	
	• EG19a	• 74	• 208	• 127.0	• 52.4*	• 3.97	• 3.97	• *I*	
	• EG19b	• 67	• 197	• 128.3	• 52.4*	• 3.76	• 3.76	• *I*	
	• EG21a	• –	• 353	• 221.1	• 201.1*	• 1.75	• 1.60	• *S*	
	• EG21b	• –	• 434	• 224.6	• 194.1*	• 2.24	• 1.93	• *S*	
• Series 4 (H = 34 cm)	• EG23a	• –	• 363	• 383.4	• 322.5*	• 1.12	• 0.95	• S_A	
	• EG23b	• –	• 386	• 375.9	• 301.2*	• 1.28	• 1.02	• S_A	
	• EG25a	• –	• 434	• 610.0	• 483.1*	• 0.90	• 0.71	• S_A	
	• EG25b	• –	• 533	• 618.9	• 515.9*	• 1.03	• 0.86	• S_A	
	• EG27a	• –	• 538	• 654.5	• 545.5*	• 0.99	• 0.82	• S_A	
	• EG27b	• –	• 686	• 658.5	• 568.6*	• 1.21	• 1.04	• S_A	
	• EG29a	• –	• 383	• 374.2	• 325.8*	• 1.18	• 1.02	• S_A	
	• EG29b	• –	• 420	• 382.3	• 341.8*	• 1.23	• 1.10	• S_A	



Note: V_I, shear force at which sliding of the interface started; V_E, shear force at structural failure; $V_{Rk,sy}$, Calculated shear resistance with lattice girders; $V_{Rk,I}$, Calculated shear resistance of the interface; *, relevant resistance (minimum of $V_{Rk,sy}$ and $V_{Rk,I}$); $V_E/V_{Rk,I}$, Ratio of maximum shear force to minimum calculated resistance; $V_E/V_{Rk,fail}$, Ratio of the maximum shear force to the calculated resistance depending on the actual failure type; S, shear failure due to yielding of the diagonal and/or vertical bars of the lattice girders; I, structural failure caused by interface failure; S_A, Shear failure due to anchorage failure of the shear reinforcement.

17517648, 0, Downloaded from https://onlinelibrary.wiley.com/doi/10.1002/suco.202200423 by Rwth Aachen Hochschulbibliothe, Wiley Online Library on [27/02/2023]. See the Terms and Conditions (https://onlinelibrary.wiley.com/terms-and-conditions) on Wiley Online Library for rules of use; OA articles are governed by the applicable Creative Commons License

3.5 | Test results

3.5.1 | General

In the following, the results of the monotonic tests on semi-precast slabs with lattice girders are presented. In addition to the structural behavior, the relevant parameters are discussed. These include the shear slenderness, the degree of shear and interface shear reinforcement, the concrete compressive strength, the slab depth, and the support detailing.

Table 6 compares the structural failure loads for the monotonic tests with the calculated load resistances for shear and interface shear according to EC2 + NA(D). For slabs where interface sliding appeared, the shear force V_I at which interface sliding began was also provided. The resistances $V_{Rk,sy}$ and $V_{Rk,I}$ in Table 6 were determined for the yield strength of $f_{yk} = 420\ N/mm^2$ to be applied according to the TA, which is intended to account for poorer bond of the diagonals due to the smooth surface of the reinforcing steel. The resistances were calculated on a characteristic level, because the roughness parameters for calculating the interface shear resistance in EC2 were derived from test data on a characteristic level.[31] Because the TA require a rough interface, the parameters for a rough interface according to Table 1 were considered in the calculated resistances $V_{Rk,I}$ for all tests where the interface was defined as almost rough. Friction was not applied for these slabs. For slabs EG 19a and EG19b, which were defined as very smooth, neither adhesion nor friction were applied.

The comparison of the shear resistances of the lattice girder $V_{Rk,sy}$ and the interface $V_{Rk,I}$ in Table 6 reveals, that, the calculated interface shear resistance is relevant for all test specimens. However, failure of the interface occurred only in test specimens EG19a and EG19b, which were designed with very smooth surfaces. All other test specimens of series 3 with a height of 16 cm showed a shear failure due to yielding of the diagonal and/or vertical bars of the lattice girders. The relative values of experimental to calculated resistances $V_E/V_{Rk,sy}$ and $V_E/V_{Rk,I}$ are clearly above 1.0 for the relevant design resistance as well as the calculated resistance depending on the cause of failure. Remarkable are the slabs EG19a and EG19b with very smooth interfaces, which reached almost four times the calculated load. This was mainly caused by the detailing of the support. The test specimens of series 4 with a height of 34 cm failed due to anchorage failure of the shear reinforcement and their failure loads are close to the calculated values. These tests in series 4 confirm the simplified reduction of the yield strength to $f_{yk} = 420\ N/mm^2$ according to the TA to account for poorer bond and anchorage (see Section 3.5.5). Since no anchorage failure of the shear reinforcement was observed for the thin slabs of series 3, an effect depending on the slab depth can be assumed.

The structural behavior under monotonic loading is explained exemplarily for test EG17a. At the beginning of the test, flexural cracks formed at the bottom of the test specimen. After increasing the load, flexural shear cracks developed from these flexural cracks (Figure 12). The deflection of the displacement-controlled test developed very uniformly until shortly before failure. After the formation of the shear cracks, the measured crack width increased over proportionately, and at the same time a strong increase in strain of the lattice girders was observed. The cause of failure was a yielding of the diagonals and verticals of the lattice girders, accompanied by a fast opening and propagation of a shear crack. The governing shear crack causing failure connected support and the position of the load introduction, which is typical for shear tests. An opening of the horizontal interface could not be observed in this test, as in the other tests except for the tests with very smooth interfaces.

Figure 13 shows the evaluation of the DIC. Based on measured crack widths and crack displacements along the crack (sliding), the alteration of the compression strut angles with increasing shear force for the two main shear cracks is determined according to a proposal of GÖRTZ[3,32] by using the crack friction model of Walraven.[33] The flexural shear cracks resulting from the flexural cracks (crack sections 1–2 and 2–2) have a crack angle of about 38 and 45°, respectively. Starting at a shear load of about 200 kN, the compression strut angle is decreasing with increasing load and is flatter than the shear crack angle at failure.

The crack opening and sliding activate aggregate interlock, which causes a concrete contribution induced by crack friction.[34] As a result, crack section 1–1 developed at about 250 kN with nearly the same inclination as the calculated compression strut inclination of crack section 1–2. This confirms the basic assumption in[34] that the direction of a new shear crack develops parallel to the compression strut. A similar behavior can be seen for crack sections 2–1.

By combining the crack pattern, the evaluated compression strut angles and the strains of the shear reinforcement, an internal redistribution process of the transfer mechanisms can be derived (Figure 14). In phase 1, flexural cracks form without shear cracks. The load transfer is similar to that in a slab without shear reinforcement. In phase 2, the first inclined cracks formed in the crack section 2–2 at a shear force of ~170 kN. With increasing load, the strains of shear reinforcement increased slightly. At the same time the crack width and sliding enlarged. However, the crack sliding was not large enough yet to generate a concrete

17517648, 0, Downloaded from https://onlinelibrary.wiley.com/doi/10.1002/suco.202200423 by Rwth Aachen Hochschulbibliothe, Wiley Online Library on [27/02/2023]. See the Terms and Conditions (https://onlinelibrary.wiley.com/terms-and-conditions) on Wiley Online Library for rules of use; OA articles are governed by the applicable Creative Commons License

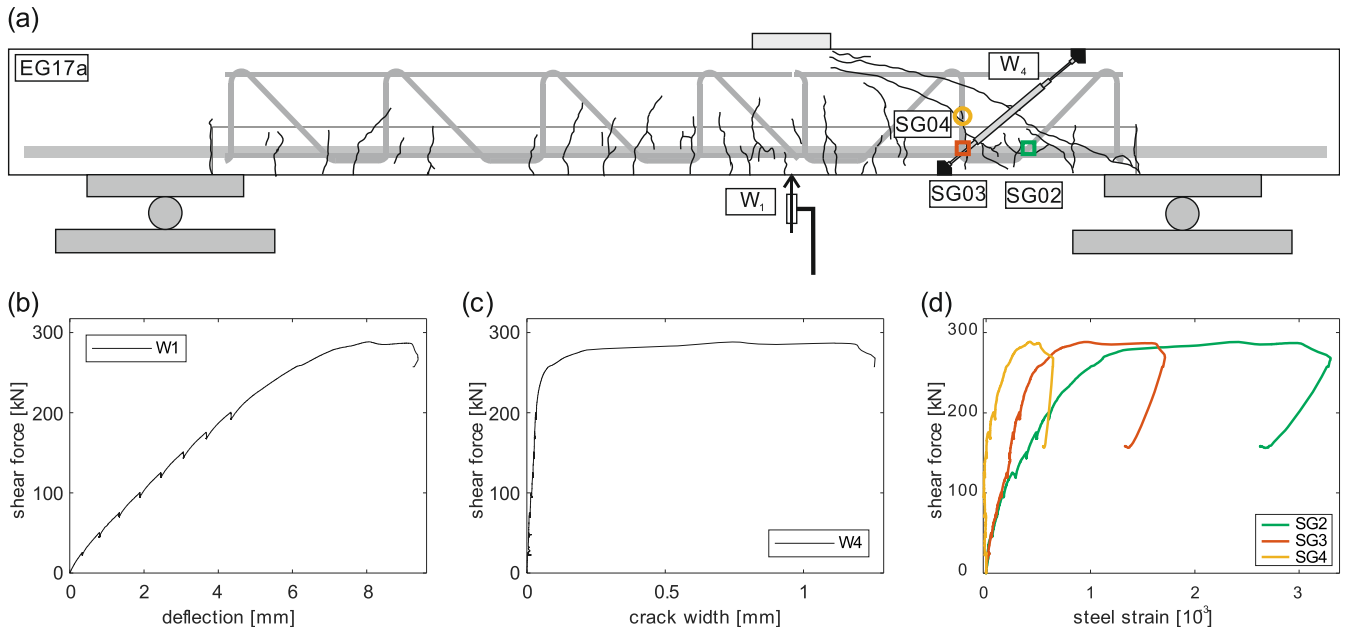


FIGURE 12 Test EG17a: (a) Crack pattern and measuring instrumentation, (b) deflection, (c) crack width, and (d) steel strains

contribution induced by aggregate interlock. The compression struts were parallel to the crack direction. In phase 3, a sufficiently large crack sliding activated crack friction, which results in compression strut inclinations smaller than the crack inclination. In the transition to phase 4, the crack width has become too large for an efficient aggregate interlock and the released force was abruptly redistributed to the shear reinforcement. The compression strut is aligned parallel to the crack again. When the shear reinforcement exceeded the yield strength, the deflections increased disproportionately and the failure occurred.

3.5.2 | Influence of shear slenderness

By comparing the tests on single-span slabs and slabs with cantilever, the influence of shear slenderness on the shear transfer was investigated. Both slabs had the same distance between load introduction and support. However, the tests result in different crack patterns and structural behaviors, as demonstrated in Figure 15.

With the single-span slab EG21a, the initial flexural cracks at the bottom side developed into flexural shear cracks, which continued to develop in direction of the load introduction. In slab EG21b with cantilever, first flexural cracks appeared at the bottom side of the slab below the load introduction simultaneously with flexural cracks at the top side, in the area of the hogging moment, which grew towards the support with increasing load (Figure 10). While the area between support and load introduction in slab EG21a was crossed by flexural and shear cracks, the shear span of slab EG21b had an almost uncracked zone between the shear cracks connecting support and load introduction until failure. In this zone, a part of the load was directly transferred into the support via a concrete compression strut. The crack shown in green in Figure 15 did not form before failure load was reached. Subsequently, no further load increase was possible.

Figure 16 compares of the measured data of tests EG21a and EG21b. With EG21a a fast increase shear crack width was observed beyond a shear force of ∼200 kN (see W4, W5). At the same time, a significant increase in steel strain was recorded at measuring point SG02 near the welding point in the lower chord of the lattice girder, which was crossed by the flexural shear crack. Under increasing load, crack width and steel strain increased rapidly until slab EG21a finally failed at a shear force of 353 kN due to yielding of the diagonal and vertical bars of the lattice girder.

Slab EG21b exhibited similar crack width up to a shear force of 200 kN at measuring point W5, however, the steel strains were significantly lower. At measuring point W4, a clear opening of the shear crack was observed not until a shear force of ∼290 kN. At this state, also the steel strain of the lattice girder at measuring point SG02 started to increase slowly. At a shear force of 434 kN, the maximum resistance of the test specimen EG21b was reached. The later shear cracking of the slab with cantilever (EG21b) can be explained by the uncracked area between the support and the load introduction, where the shear force was transferred directly into the support via a compression strut.

17517648, 0, Downloaded from https://onlinelibrary.wiley.com/doi/10.1002/suco.202200423 by Rwth Aachen Hochschulbibliothe, Wiley Online Library on [27/02/2023]. See the Terms and Conditions (https://onlinelibrary.wiley.com/terms-and-conditions) on Wiley Online Library for rules of use; OA articles are governed by the applicable Creative Commons License

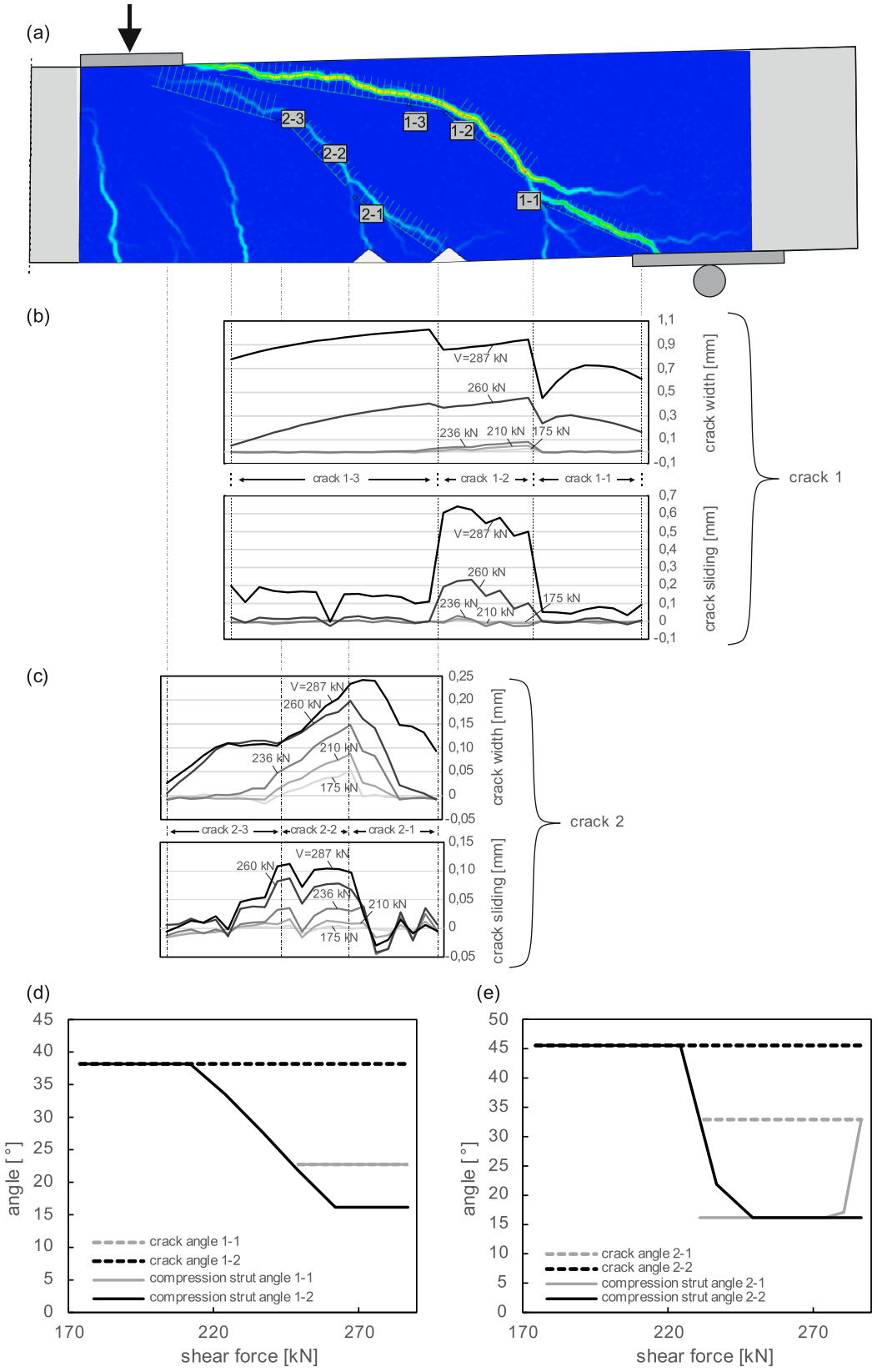


FIGURE 13 Test EG17a: Evaluation of the digital image correlation with (a) crack pattern, (b,c) crack width and sliding along the crack for different shear load stages, and (d,e) development of the determined compression strut angle per crack

17517648, 0, Downloaded from https://onlinelibrary.wiley.com/doi/10.1002/suco.202200423 by Rwth Aachen Hochschulbibliothe, Wiley Online Library on [27/02/2023]. See the Terms and Conditions (https://onlinelibrary.wiley.com/terms-and-conditions) on Wiley Online Library for rules of use; OA articles are governed by the applicable Creative Commons License

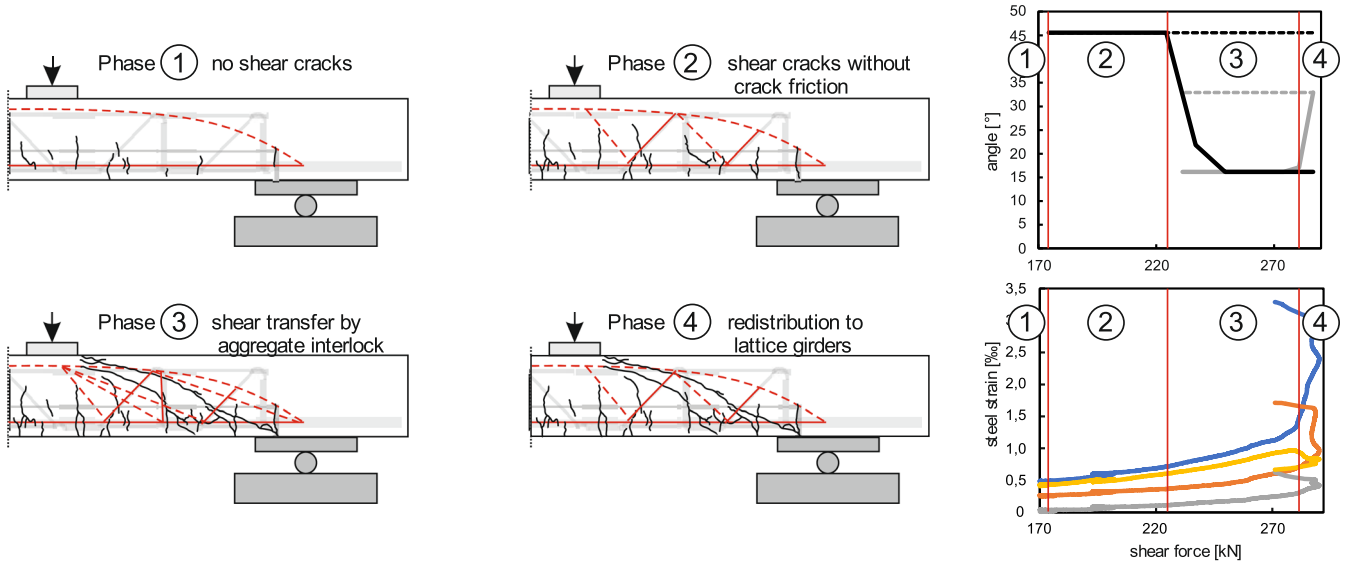


FIGURE 14 Test EG17a: Redistribution process of the shear transfer mechanisms

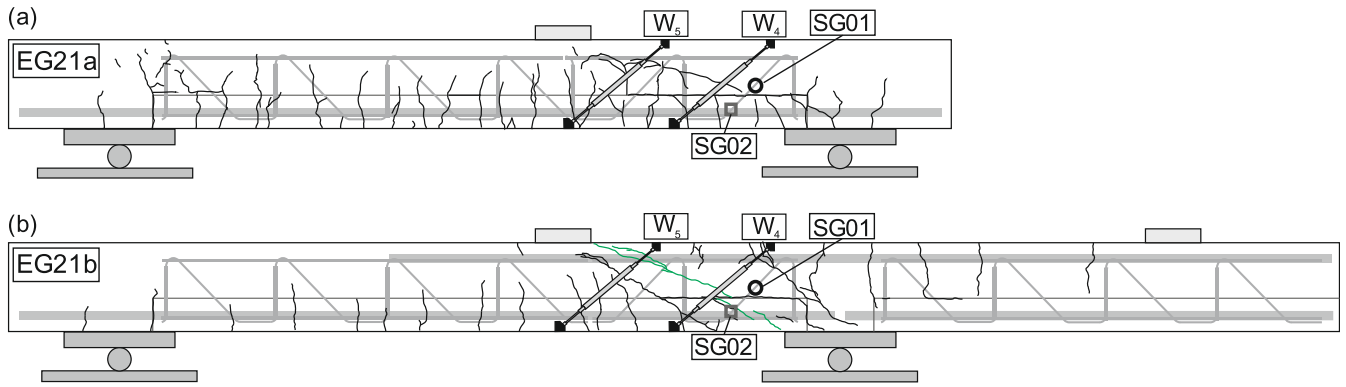


FIGURE 15 Crack patterns of (a) EG21a and (b) EG21b

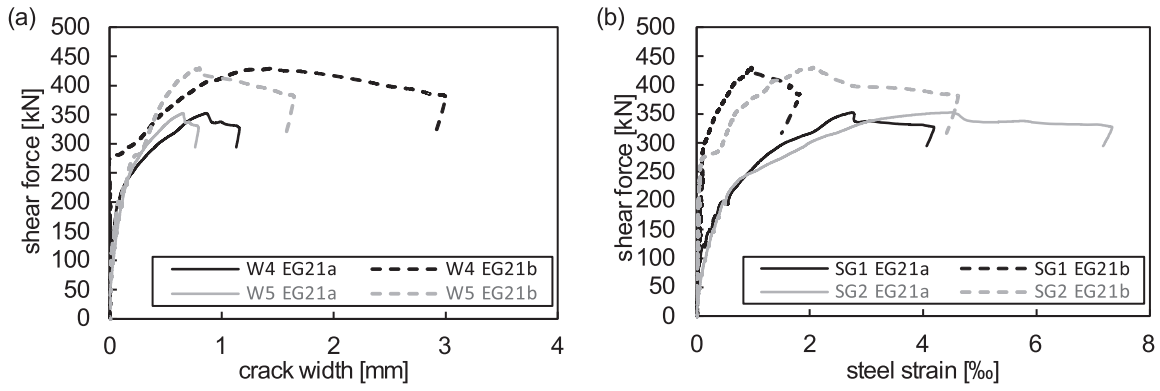


FIGURE 16 Comparison of (a) crack widths and (b) steel strains of slabs EG21a and EG21b

Figure 17 compares the normalized shear resistances between single-span slabs and slabs with cantilever. All slabs with a cantilever with an almost rough interface reached a between 6% and 27% higher shear resistance at the inner support compared to a test at the end support with the same load distance. Basically, the test results confirm that specimens with smaller shear slenderness gain a higher shear resistance due to a different shear

17517648, 0, Downloaded from https://onlinelibrary.wiley.com/doi/10.1002/suco.202200423 by Rwth Aachen Hochschulbibliothe, Wiley Online Library on [27/02/2023]. See the Terms and Conditions (https://onlinelibrary.wiley.com/terms-and-conditions) on Wiley Online Library for rules of use; OA articles are governed by the applicable Creative Commons License

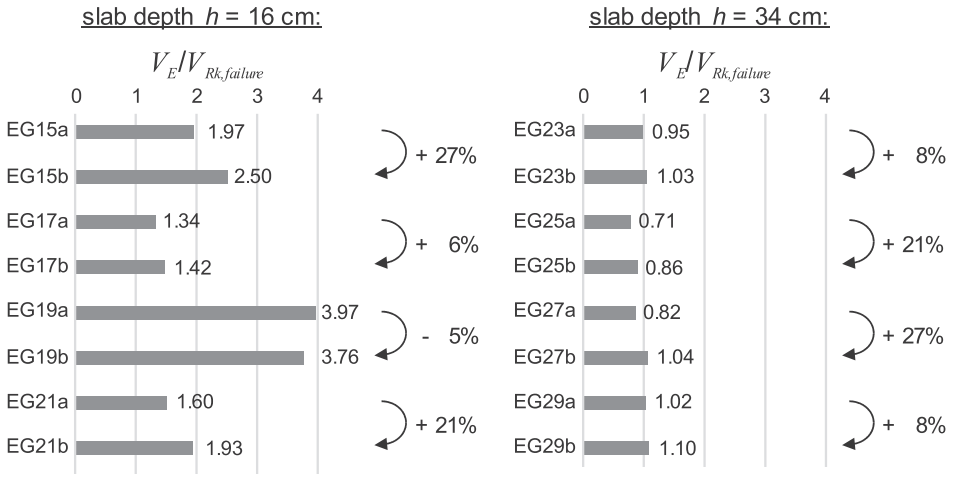


FIGURE 17 Influence of the shear slenderness: comparison of normalized shear resistance ($V_E/V_{Rk,fail}$) between single-span slabs ($\lambda = 4.0$; e.g., EG15a) and slabs with cantilever ($\lambda = 2.5$; e.g., EG15b)

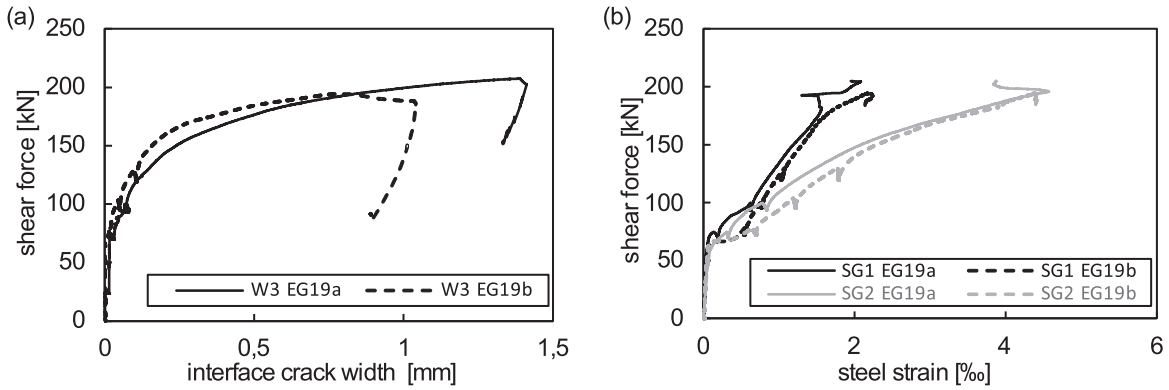


FIGURE 18 (a) Interface crack width and (b) steel strains of slabs EG19a and EG19b

cracking behavior and a load transfer via a direct compression strut into the support.

The lower shear resistance of test specimen EG19b in comparison to EG19a can be explained by the failure of the very smooth interface. In both test specimens, an opening of the interface was measured at low shear forces of 60–70 kN (Figure 18). At the same time, the strains of the lattice girders increased abruptly. In both tests, displacement of the in situ concrete was prevented. At the inner support, displacement was impeded by the adjacent field, and at the end support by the detailing of the support used here (Section 3.5.6). Compared to the support detail of an end support according to Figure 5c, where a displacement of the in-situ concrete and thus an earlier interface shear failure is possible, an increase in interface shear resistance is expected at the inner support. Test results with monotonic loading and detailing of support according to Figure 5c are not available. Therefore, the higher shear resistance at the inner support depends not only on the shear slenderness but also on the roughness of the interface, the detailing of the support, and the type of failure.

Other influencing parameters for the increase in resistance for slabs with almost rough interfaces could not be conclusively determined from the tests carried out. The higher resistance at the inner support can be explained by a larger concrete contribution $V_{Rd,cc}$ in Equation (2), which is governed by the shear slenderness. A similar approach was proposed in Hegger et al.[3] for slabs with low shear reinforcement ratios.

3.5.3 | Influence of the shear reinforcement ratio

Basically, slabs with higher shear or interface shear reinforcement ratios gained a higher load than those with low shear reinforcement ratios (see Table 6). A comparison of the normalized shear resistance $V_E/V_{Rk,fail}$ reveals that the design according to Equation (1) underestimates the concrete contribution (Figure 19). In particular, thin slabs with a low shear reinforcement ratio significantly exceed the expected calculated resistances.

17517648, 0, Downloaded from https://onlinelibrary.wiley.com/doi/10.1002/suco.202200423 by Rwth Aachen Hochschulbibliothe, Wiley Online Library on [27/02/2023]. See the Terms and Conditions (https://onlinelibrary.wiley.com/terms-and-conditions) on Wiley Online Library for rules of use; OA articles are governed by the applicable Creative Commons License

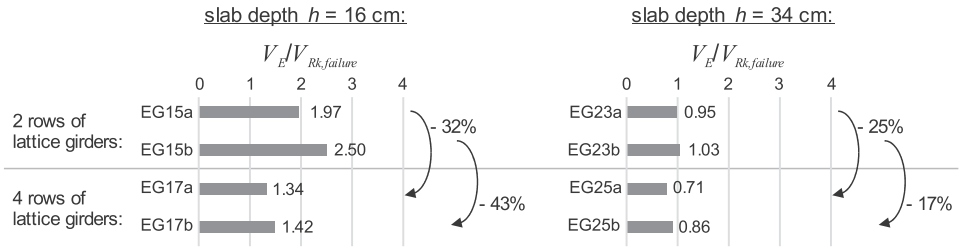


FIGURE 19 Influence of the reinforcement ratio: comparison of the normalized shear resistance ($V_E/V_{Rk,fail}$)

TABLE 7 Influence of the concrete compressive strength on the absolute shear resistance

Test C25/30|C50/60	V_E [kN] C25/30	C50/60	$V_{E,C50/60}/V_{E,C25/30}$
EG17a|EG21a	288	353	1.23
EG17b|EG21b	293	434	1.48
EG25a|EG27a	434	538	1.24
EG25b|EG27b	533	686	1.29

3.5.4 | Influence of concrete compressive strength

To investigate the influence of the concrete compressive strength the minimum and maximum values according to TA (C25/30 and C50/60, respectively) for identical slabs were used.

As expected, a lower shear resistance was found for the slabs with lower concrete strength. On average, the absolute resistance was increased by 23%–48% by doubling the concrete strength (Table 7). An evaluation of the normalized shear capacity reveals that the design (Equation (1)), however, still underestimates high concrete strengths (increase of 16%–36%, Figure 20).

3.5.5 | Influence of the slab depth

The thin slabs of series 3 reached significantly higher maximum loads compared to the calculated resistances (Table 6). This leads to the assumption that there is a dependence of shear capacity on the slab depth.

Basically, the development of crack pattern during the test was not different between thin and thick slabs (Figure 21). But just before failure, the shear crack developed horizontally along the flexural reinforcement for the thick slabs with $h = 34$ cm. The structural behavior at this stage was highly dependent on the dowel action. Similar findings were reported in Adam[2] for slabs without shear reinforcement. In some thick slabs, an almost continuous horizontal splitting of the test specimen occurred at the level of the longitudinal reinforcement, which led to failure. This cracking pattern with horizontal splitting was also observed in the cyclic tests in the previous project.[25] In the case of thin slabs, a part of a crack also developed along the flexural reinforcement in the direction of the support, but this crack had a comparatively small crack width and was not decisive for the failure as splitting could not be detected.

A further investigation illustrates that the dowel action was more pronounced in the thick slabs, since the anchorage of the vertical and diagonal lattice girder bars could not bear any further force. By transforming the formulas for shear design according to EC2 + NA (D) (Equations (1) and (2)), the theoretical compression strut angle for slab EG23a can be determined to be ∼26° (Figure 22a), which is accompanied with an ∼55 cm wide tension strut. This corresponds to about five bars of the lattice girder as shear reinforcement in each element. According to the strain measurement of the shear reinforcement, one diagonal bar (measurement point SG05) exceeded the yield strain of the reinforcing steel of 2.5‰ (Figure 22c). While the strains of adjacent bars are lower and, therefore, contributed less to the shear capacity. Figure 22d shows the lattice girder in the failure zone after removing the concrete. Larger deformations can be seen on the upper and lower chords of the lattice girders around the welding points, indicating that the nodes were pulled out of their original position. As a result, the bars could not increase the contribution to the shear capacity. In contrast, no deformations and no anchorage failure can be detected for the part of the lattice girder with measurement point SG05. This diagonal bar reaches the yield strain. On average, the simultaneous yielding of the steel and partially slippage of the anchorage of the lattice girders is covered in the calculation by taking into account the simplified reduction of the yield strength of lattice girders to $f_{yk} = 420$ N/mm^2 specified in the TA.

The deformations at the chords of the lattice girder could only be detected in slabs of series 4. Besides the slab thickness, there is a decisive influence of the lattice girder geometry. With increasing slab thickness the inclination of the diagonal bars are becoming steeper (Figure 4). With steeper diagonals, the anchorage is additionally loaded. Further investigations are required to explain this influence more in detail.

17517648, 0, Downloaded from https://onlinelibrary.wiley.com/doi/10.1002/suco.202200423 by Rwth Aachen Hochschulbibliothe, Wiley Online Library on [27/02/2023]. See the Terms and Conditions (https://onlinelibrary.wiley.com/terms-and-conditions) on Wiley Online Library for rules of use; OA articles are governed by the applicable Creative Commons License

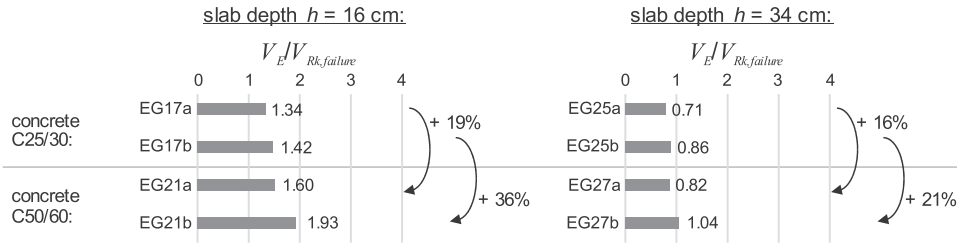


FIGURE 20 Influence of concrete compressive strength: comparison of the normalized shear resistance between low (e.g., EG17a) and high concrete compressive strength (e.g., EG21a)

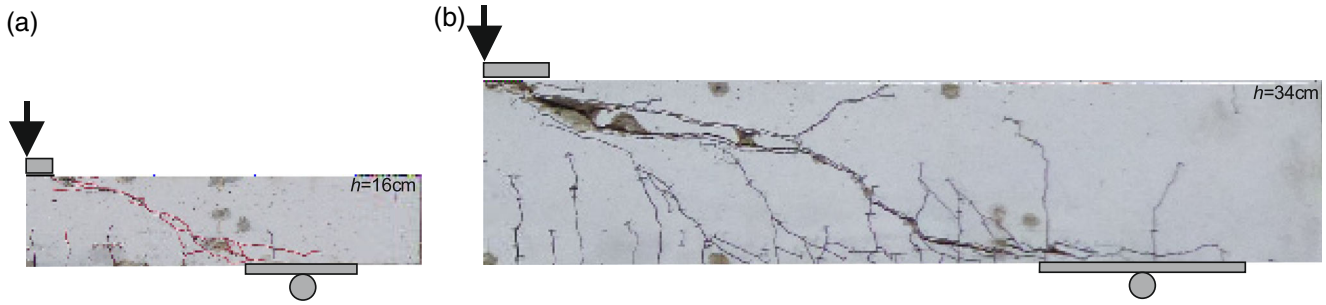


FIGURE 21 Comparison of crack patterns of slabs (a) EG15a and (b) EG23a

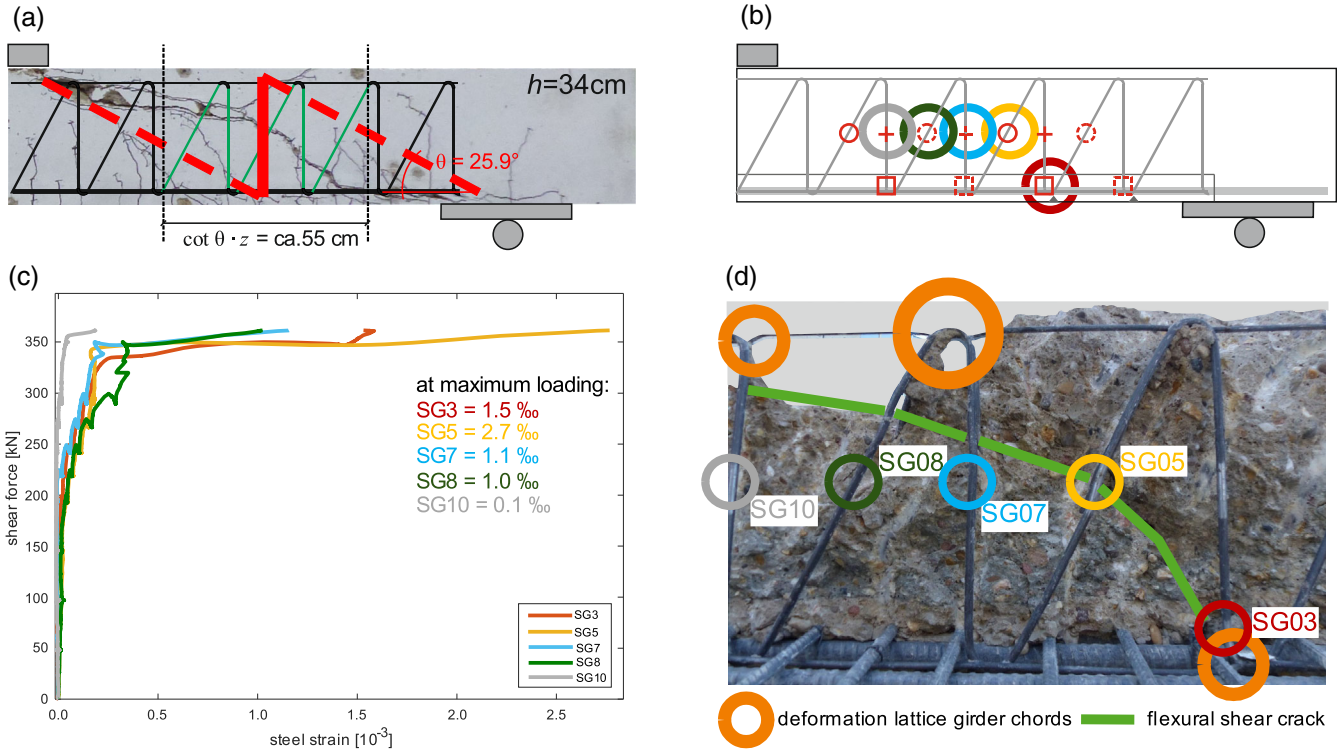


FIGURE 22 Investigation of the failure of test EG23a

3.5.6 | Influence of interface roughness and detailing of the support

In all tests with an almost rough interface, an opening and sliding of the horizontal interface were not observed, as already demonstrated by the example of slab EG17a (Figure 12). In contrast to the previous project in Hegger and Wieneke,[25] the horizontal interface was not realized along the entire length of the slab (Figure 5).

The support detailing according to Figure 5d in the current test series had a positive effect on the shear as well as the interface shear resistance of the semi-

17517648, 0, Downloaded from https://onlinelibrary.wiley.com/doi/10.1002/suco.202200423 by Rwth Aachen Hochschulbibliothe, Wiley Online Library on [27/02/2023]. See the Terms and Conditions (https://onlinelibrary.wiley.com/terms-and-conditions) on Wiley Online Library for rules of use; OA articles are governed by the applicable Creative Commons License

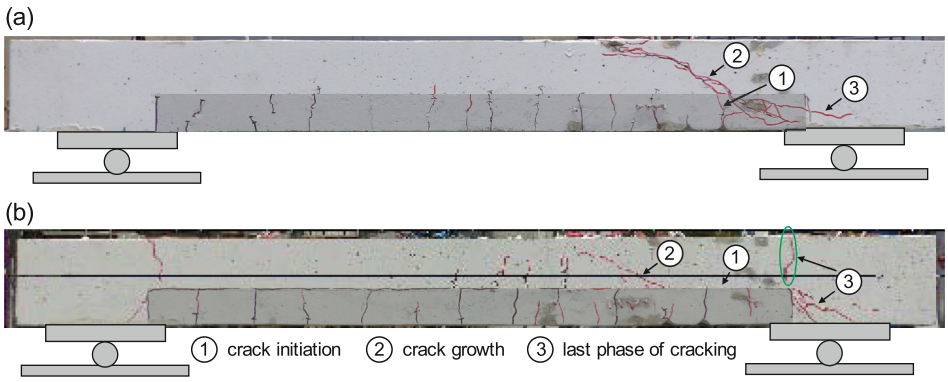


FIGURE 23 Crack patterns of tests (a) EG15a (almost rough interface) and (b) EG19a (very smooth interface)

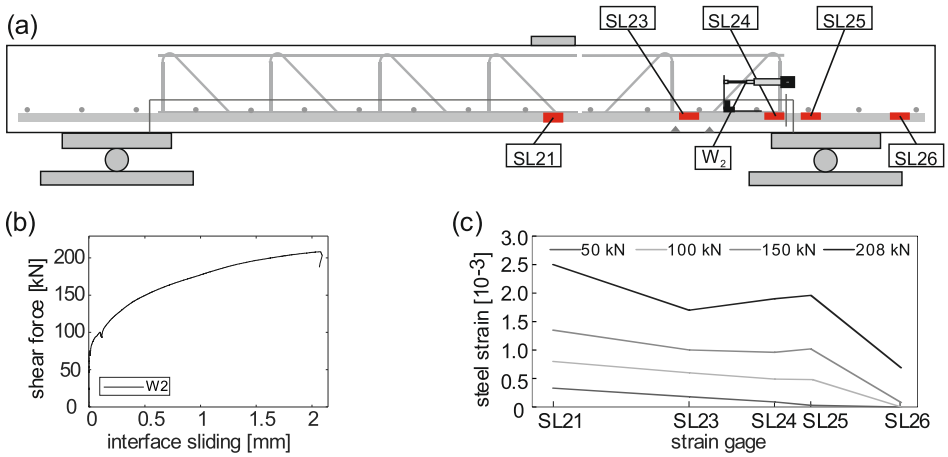


FIGURE 24 EG19a: (a) Measuring instrumentation, (b) interface sliding, and (c) strain of longitudinal reinforcement

precast slabs. To evaluate the effect of the support detailing, the slabs EG19a and EG19b were designed with a very smooth surface, which provoked an opening of the horizontal interface. The comparison between V_I and $V_{Rk,I}$ (Table 6) for these slabs shows that the start of the interface sliding occurred at an about 30%–40% higher shear force than calculated. Although the very smooth interface resulted in an opening and sliding on the entire interface length, a structural failure due to shearing off the interface still did not occur.

A comparison of the crack patterns of slabs EG15a and EG19a (Figure 23), which were identical except for the interface roughness, confirms that the shear crack creating failure in slab EG15a developed from a flexural crack near the support to the point of the load introduction. In slab EG19a, the shear cracks were influenced by the interface cracking. Because of the very smooth interface, a vertical crack was located in the area of the support in extension of the vertical interface between the prefabricated slab and the in situ concrete in slab EG19a (Figure 23, green mark).

As can be seen in Figure 24, the interface sliding in EG19a increased to more than 2 mm at the end of the test, which indicates an interface failure Mutual displacements beyond this may be limited by the detailing of the support. Toward the end of the test, the vertical cracks on the top side formed, which can be attributed to the interface sliding and the anchorage of the longitudinal reinforcement. While the interface sliding increased continuously the in situ concrete layer was pushed outwards, and the longitudinal reinforcement anchored in the in situ concrete generated an arching effect (Figure 25).

The arching effect is also confirmed by the increased strains of the longitudinal reinforcement at the support. The strain under maximum load underneath the load introduction was 2.5‰ (SL21, Figure 24). Toward the support, this strain initially decreased according to the moment and was only ∼1.7‰ (SL23) within the shear span. However, in the vertical interface between the prefabricated slab and the in situ concrete, the strain in the longitudinal reinforcement was higher [∼1.95‰ (SL25)] due to arching.

Due to the anchorage of the longitudinal reinforcement in the in situ concrete, on the one hand, a horizontal shearing of the top concrete from the semi-precast slab and thus an early failure was prevented and on the other hand, the favorable arching effect was enabled. Despite of visible failure of the interface, the shear

17517648, 0, Downloaded from https://onlinelibrary.wiley.com/doi/10.1002/suco.202200423 by Rwth Aachen Hochschulbibliothe, Wiley Online Library on [27/02/2023]. See the Terms and Conditions (https://onlinelibrary.wiley.com/terms-and-conditions) on Wiley Online Library for rules of use; OA articles are governed by the applicable Creative Commons License

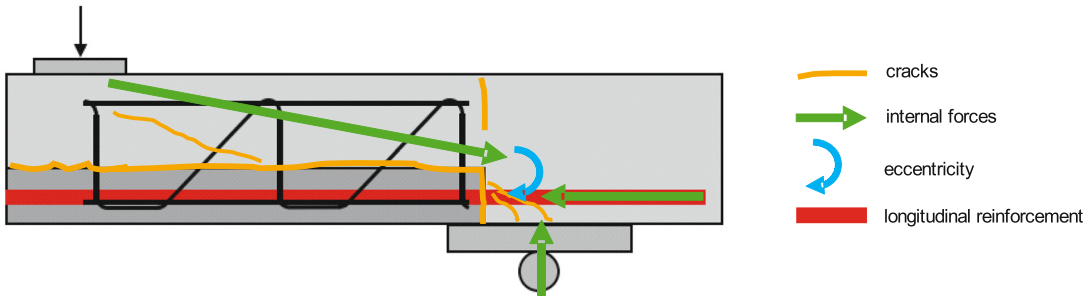


FIGURE 25 EG19a: Shear transfer by arching effect due to in situ concrete

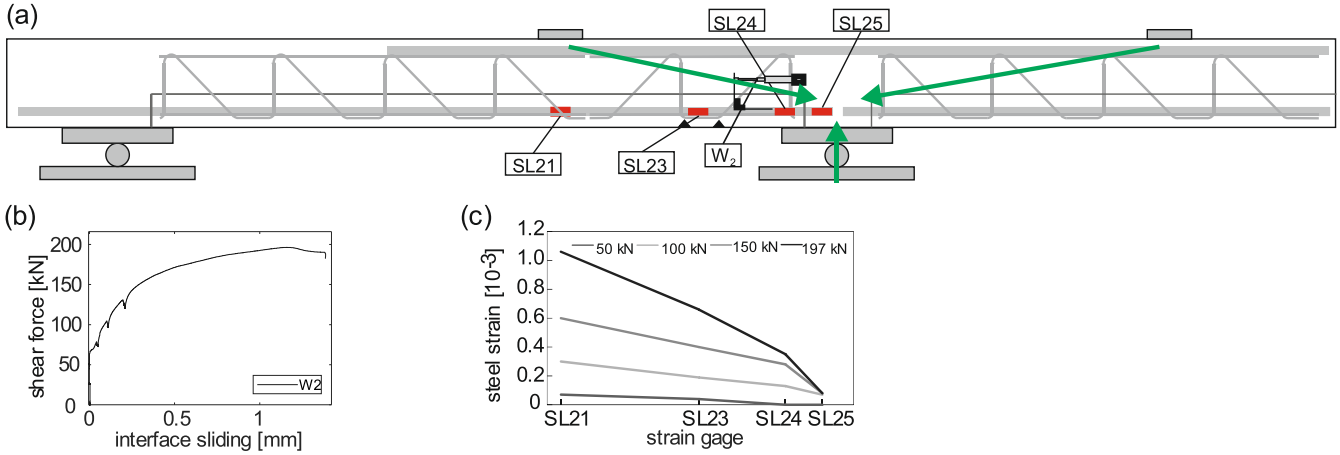


FIGURE 26 EG19b: (a) Measuring instrumentation, (b) interface sliding, and (c) strain of longitudinal reinforcement

capacity at structural failure was almost four times higher than the calculated interface shear resistance. In comparison, interface failure in a slab with a very smooth interface provided along the entire slab, as tested in Hillebrand et al. and Hegger and Wieneke[5,25] and shown in (Figure 5c), corresponds directly to structural failure. Therefore, in addition to adhesion, friction, and interface reinforcement (Equation (5)), an additional contribution dependent on the detailing of the slab at the support area should be considered. Further research is needed to define this contribution, but a failure of the interface is less likely to be decisive when the support is constructed as shown in Figure 25.

For test specimen EG19b (slab with cantilever), the favorable effect of a well-anchored longitudinal reinforcement in the in-situ concrete was not necessary. Below load introduction, the largest strain of ~1‰ was measured at the end of the test, while the strain decreased to ~0.7‰ in the shear span (Figure 26). In contrast to test specimen EG19a, there was no higher strain at the inner support in the very short anchorage length of the longitudinal reinforcement. However, the favorable arching effect was generated by the compression strut of the adjacent span of the continuous slab. The failure load of test EG19b was nearly the same as in test EG19a.

4 | SUMMARY

Semi-precast slabs consisting of a prefabricated slab element with lattice girders and an in situ concrete layer are a very economical construction method for buildings. Theoretical and experimental investigations were carried out to describe the structural behavior for shear and interface shear of semi-precast slabs with lattice girders under monotonic loading. The main parameters of the study were shear slenderness, shear reinforcement ratio, concrete strength, slab depth as well as detailing of the support area.

The theoretical and experimental findings of 16 tests under monotonic loading can be summarized as follows:

- For thin slabs (16 cm) with lattice girders, the experimental resistance significantly exceeded the calculated shear resistance, while the shear capacity of the thick slabs (34 cm) roughly corresponded to the calculated resistance. Anchorage failure of the lattice girders was observed in some thick slabs, confirming the reduced yield strength for lattice girders specified in the TA.
- All tests with an almost rough interface failed by bending shear failure without any crack along the interface.

17517648, 0, Downloaded from https://onlinelibrary.wiley.com/doi/10.1002/suco.202200423 by Rwth Aachen Hochschulbibliothe, Wiley Online Library on [27/02/2023]. See the Terms and Conditions (https://onlinelibrary.wiley.com/terms-and-conditions) on Wiley Online Library for rules of use; OA articles are governed by the applicable Creative Commons License

Only in tests with a very smooth interface a separation between the precast slab and the in situ concrete was observed.

- For slabs with very smooth interface, however, the experimental failure load was significantly higher than the calculated resistance according to Eurocode 2, despite the clearly visible interface crack. This was mainly caused by the detailing of the support. With a short support length of the precast element and a sufficient anchorage length of the longitudinal reinforcement in the in situ concrete a favorable arching effect is generated. This additional contribution, which is only possible with this type of support detailing, increases the interface shear resistance.
- Comparisons of the normalized shear resistance show that the current design underestimates the concrete contribution as well as high concrete strengths.
- The comparison of single-span slabs with continuous slabs confirmed that the shear and interface shear resistance at the inner support are increased compared to an end support. Since the shear resistance of semi-precast slabs with low shear reinforcement ratios consists of a concrete contribution and a contribution of the shear reinforcement, the smaller shear slenderness at the inner support of a continuous slab increased shear capacity.

These findings illustrate further potential for improvements in the design of semi-precast slabs with lattice girders under monotonic loading. Further investigations are required to quantify all favorable effects in order to improve the economic efficiency. As the design rules for fatigue lead currently to uneconomical results as well, related tests with cyclic loading will be presented in an upcoming publication.

ACKNOWLEDGMENTS

The investigations described in this paper are conducted during a research program initiated by the Research Association of the German Concrete and Precast Industry e. V. and funded by the German Federation of Industrial Research Association (AiF, IGF number 20580 N) and the Federal Ministry for Economic Affairs and Climate Action based on a resolution of the German Bundestag. The authors express their thanks to the sponsors and the members of the project committee for the constructive discussions. Open access funding enabled and organized by Projekt DEAL.

DATA AVAILABILITY STATEMENT

The data that support the findings of this study are available from the corresponding author upon reasonable request.

ORCID

Matthias Hillebrand https://orcid.org/0000-0001-8215-9987

Josef Hegger https://orcid.org/0000-0003-3066-5006

REFERENCES

1. Furche J, Bauermeister U. Elementbauweise mit Gitterträgern. In: Bergmeister K, Fingerloos F, Wörner J-D, editors. Beton-Kalender 2021: Schwerpunkte: Fertigteile; Integrale Bauwerke. 1st ed. Berlin: Ernst & Sohn; 2021.
2. Adam V. Shear in reinforced concrete structures without shear reinforcement—analysis and design [dissertation]. Aachen: RWTH Aachen University; 2021.
3. Hegger J, Sherif A, Görtz S. Investigation of pre- and postcracking shear behavior of prestressed concrete beams using innovative measuring techniques. ACI SJ. 2004;101:183–92.
4. Furche J, Bauermeister U, Kummerow A, Hillebrand M. Durchstanzen bei Ermüdungsbeanspruchung. BuSt. 2019;87:216. https://doi.org/10.1002/best.201900012
5. Hillebrand M, Schmidt M, Wieneke K, Classen M, Hegger J. Investigations on Interface shear fatigue of semi-precast slabs with lattice girders. Appl Sci. 2021;11:11196. https://doi.org/10.3390/app112311196
6. Filigran Trägersysteme GmbH & Co. KG. Allgemeine bauaufsichtliche Zulassung Z-15.1-93: Filigran-EQ-Gitterträger für Fertigplatten mit statisch mitwirkender Ortbetonschicht. Berlin: Filigran Trägersysteme GmbH; 2019.
7. Badische Drahtwerke GmbH. Allgemeine bauaufsichtliche Zulassung Z-15.1-38: Kaiser-Omnia-Träger KTS für Fertigplatten mit statisch mitwirkender Ortbetonschicht. Berlin: Badische Drahtwerke GmbH; 2020.
8. Deutsches Institut für Normung e.V. (DIN). Eurocode 2: Design of concrete structures—Part 1-1: General rules and rules for buildings: German version EN 1992-1-1:2004 + AC: 2010, 91.010.30–91.080.40. Berlin: Beuth; 2011.
9. Deutsches Institut für Normung e.V. (DIN). National Annex—nationally determined parameters—Eurocode 2: design of concrete structures—part 1-1: general rules and rules for buildings; 91.080.40. Berlin: Beuth; 2013.
10. Leonhardt F, Walther R. The Stuttgart Shear Tests: Contributions to the treatment of the problems of shear in reinforced concrete construction. Cem Concr Ass. 1961;1964:111.
11. Kani GNJ. The riddle of shear failure and its solution. J Amer Conc Inst. 1964;61:441–67. https://doi.org/10.14359/7791
12. Islam MS, Pam HJ, Kwan A. Shear capacity of high strength concrete beams with their point of inflection within the shear span. Proc Inst Civil Eng Struct Buil. 1998;128:91–9.
13. Taylor SE, Rankin GIB, Cleland DJ. Guide to Compressive Membrane Action. Surrey, UK: Concrete Bridge Development Group; 2001.
14. Yang Y. Shear behaviour of reinforced concrete members without shear reinforcement: a new look at an old problem [dissertation]. Delft: Delft University of Technology; 2014.
15. Fernández Ruiz M, Muttoni A, Sagaseta J. Shear strength of concrete members without transverse reinforcement: a mechanical approach to consistently account for size and strain effects. Eng Struct. 2015;99:360–72. https://doi.org/10.1016/j.engstruct.2015.05.007

17517648, 0, Downloaded from https://onlinelibrary.wiley.com/doi/10.1002/suco.202200423 by Rwth Aachen Hochschulbibliothe, Wiley Online Library on [27/02/2023]. See the Terms and Conditions (https://onlinelibrary.wiley.com/terms-and-conditions) on Wiley Online Library for rules of use; OA articles are governed by the applicable Creative Commons License

16. Tue NV, Tung ND. Study on the influence of M/V-combination on the shear behaviour of slender reinforced concrete beams without stirrups. In: Bayrak O, Fernández Ruiz M, Kaufmann W, Muttoni A, editors. Towards a rational understanding of shear in beams and slabs: fib bulletin 85: workshop in Zürich. Fédération Internationale du Béton (fib): Switzerland; 2018. p. 100–20.
17. Classen M. Shear crack propagation theory (SCPT) – the mechanical solution to the riddle of shear in RC members without shear reinforcement. Eng Struct. 2020;210:110207. https://doi.org/10.1016/j.engstruct.2020.110207
18. Adam V, Classen M, Hillebrand M, Hegger J. Shear in continuous slab segments without shear reinforcement under distributed loads. In: Derkowski W, Gwozdziewicz P, Hojdys L, Krajewski P, Pantak M, editors. Fib symposium. Krakow, Poland: International Federation for Structural Concrete; 2019. p. 1771–8.
19. Leonhardt F, Walther R, Dilger W. Schubversuche an Durchlaufträgern (Zweifeldrige Stahlbetonbalken mit und ohne Schubbewehrung): DAfStb-Heft 163. Berlin: Ernst & Sohn; 1964.
20. Herbrand M, Hegger J. Experimentelle Untersuchungen zum Einfluss einer externen Vorspannung auf die Querkrafttragfähigkeit vorgespannter Durchlaufträger. Bauingenieur. 2013;88:428–37.
21. Maurer R, Gleich P, Zilch K, Dunkelberg D. Querkraftversuch an einem Durchlaufträger aus Spannbeton. Beton-Und Stahlbetonbau. 2014;109:654–65. https://doi.org/10.1002/best.201400054
22. Teworte F, Herbrand M, Hegger J. Structural assessment of concrete bridges in Germany—shear resistance under static and fatigue loading. Struc Eng Int. 2015;25:266–74. https://doi.org/10.2749/101686615X14210663188411
23. Gleich P, Maurer R. An analytical model to determine the shear capacity of prestressed continuous concrete beams. IABSE Congress, Stockholm 2016: challenges in design and construction of an innovative and sustainable built environment. Stockholm, Sweden: International Association for Bridge and Structural Engineering (IABSE) Zurich; 2016. p. 1544–55. https://doi.org/10.2749/stockholm.2016.1539
24. Herbrand M. Shear strength models for reinforced and prestressed concrete members [dissertation]. Aachen: RWTH Aachen University; 2017.
25. Hegger J, Wieneke K. Ermüdung von Elementdecken mit Gitterträgern: Abschlussbericht zum IGF-Forschungsvorhaben 18407 N/1. Aachen: RWTH Aachen University; 2017.
26. Riedel P, Leutbecher T. Shear bearing behaviour of slender reinforced concrete members without shear reinforcement containing a low ratio of longitudinal reinforcement. In: Hordijk DA, Luković M, editors. Fib symposium. Cham: Springer International Publishing; 2017. p. 710–8. https://doi.org/10.1007/978-3-319-59471-2_84
27. Hegger J, Hillebrand M. Ermüdung von Elementdecken mit Gitterträgern an Einfeld- und Durchlaufträgern: Abschlussbericht zum IGF-Forschungsvorhaben 20580 N/1. Aachen: RWTH Aachen University; 2022.
28. Kaufmann N. Das Sandflächenverfahren. Strassenbau-Technik. 1971;24:131–5.
29. Wieneke K, Herbrand M, Vogler N, Schwermann R, Blankenbach J. Messverfahren zur Bestimmung der Rautiefe von Betonoberflächen. Bauingenieur. 2018;93:365–73. https://doi.org/10.37544/0005-6650-2018-09-65
30. GOM GmbH. GOM correlate professional. Braunschweig, Germany: GOM GmbH; 2019.
31. Wieneke KM. Horizontal shear design of concrete interfaces in beam and slab structures [dissertation]. Aachen: RWTH Aachen University; 2019.
32. Görtz S. Zum Schubrissverhalten von Stahlbeton- und Spannbetonbalken aus Normal- und Hochleistungsbeton [Dissertation]. Aachen: RWTH Aachen; 2004.
33. Walraven JC. Aggregate interlock: a theoretical and experimental analysis [PhD thesis]. Delft, Netherlands: Delft University of Technology; 1980.
34. Reineck K-H. Hintergründe zur Querkraftbemessung in DIN 1045-1 für Bauteile aus Konstruktionsbeton mit Querkraftbewehrung. Bauingenieur. 2001;76:168–79.

AUTHOR BIOGRAPHIES



Matthias Hillebrand, RWTH Aachen University, Institute of Structural Concrete, Mies-van-der-Rohe-Str 1, 52074 Aachen, Germany. Email: mhillebrand@imb.rwth-aachen.de.



Josef Hegger, RWTH Aachen University, Institute of Structural Concrete, Mies-van-der-Rohe-Str 1, 52074 Aachen, Germany. Email: jhegger@imb.rwth-aachen.de.

How to cite this article: Hillebrand M, Hegger J. Shear and interface shear of semi-precast slabs with lattice girders under monotonic loading. Structural Concrete. 2023. https://doi.org/10.1002/suco.202200423

17517648, 0, Downloaded from https://onlinelibrary.wiley.com/doi/10.1002/suco.202200423 by Rwth Aachen Hochschulbibliothe, Wiley Online Library on [27/02/2023]. See the Terms and Conditions (https://onlinelibrary.wiley.com/terms-and-conditions) on Wiley Online Library for rules of use; OA articles are governed by the applicable Creative Commons License